TECHNISCHE UNIVERSITÄT WIEN

DIPLOMARBEIT

Stabilization of Spin Ensembles in Hybrid Quantum Systems

zur Erlangung des akademischen Grades

Diplom-Ingenieur

im Rahmen den Studiums

066 461 Masterstudium Technische Physik

ausgeführt am Institut für Theoretische Physik
der Technischen Universität Wien

unter der Anleitung von
Univ.Prof. Dipl.-Ing. Dr.techn. Stefan Rotter
und
Dipl.-Ing. Dr.techn. Matthias Zens
durch

Tobias Reiter
[redacted]

Datum _____ Unterschrift _____

Die approbierte gedruckte Originalversion dieser Diplomarbeit ist an der TU Wien Bibliothek verfügbar
The approved original version of this thesis is available in print at TU Wien Bibliothek.

Die approbierte gedruckte Originalversion dieser Diplomarbeit ist an der TU Wien Bibliothek verfügbar
The approved original version of this thesis is available in print at TU Wien Bibliothek.

Abstract

Hybrid quantum systems play an eminent role in the development of modern quantum information technology. They combine the advantages of complementary quantum systems, e.g., by using photons for transmitting quantum information and spins as long-lived quantum memories. Promising candidates in this regard are solid state spin ensembles coupled to a cavity, such as nitrogen-vacancy centers in diamond, which we consider in this thesis. In particular, we focus on inverted spin ensembles, which tend to be unstable systems, releasing their stored energy into the cavity. Being able to stabilize such an inverted spin ensemble enables a host of practical applications in modern quantum information technology ranging from quantum memories and quantum batteries to highly sensitive photo-detectors.

In this thesis, we study various stabilization mechanisms for inverted spin ensembles coupled to a single cavity mode. First, we introduce a method of static stabilization, based on the inhomogeneous broadening and collective cooperativity of the ensemble. Here, we present a general framework, which allows us to determine a criterion for the stability of the inverted spin ensemble.

We then extend this framework to periodically modulated systems by utilizing Floquet theory, which lets us determine a condition for stability with the help of the one-period propagator. While our derived formalism is very general, we test our dynamic stabilization method by simulating the dynamics of a concrete physical realization, based on nitrogen-vacancy centers in diamond. In this context, we also investigate the effect of an external probing pulse applied to a stabilized spin system. Finally, we study the stabilization mechanism in more detail, revealing a connection between stabilization and the phases of the cavity field and spins.

Die approbierte gedruckte Originalversion dieser Diplomarbeit ist an der TU Wien Bibliothek verfügbar
The approved original version of this thesis is available in print at TU Wien Bibliothek.

Die approbierte gedruckte Originalversion dieser Diplomarbeit ist an der TU Wien Bibliothek verfügbar
The approved original version of this thesis is available in print at TU Wien Bibliothek.

Zusammenfassung

Hybride Quantensysteme spielen eine wichtige Rolle bei der Entwicklung der modernen Quanteninformationstechnologie. Sie vereinen die Vorteile komplementärer Quantensysteme, indem sie z. B. Photonen zur Übertragung von Quanteninformation und Spins als langlebige Quantenspeicher nutzen. Vielversprechende Kandidaten in dieser Hinsicht sind Festkörper-Spin-Ensembles, die an einen Resonator gekoppelt sind, wie z. B. Stickstoff-Fehlstellen in Diamant, die wir in dieser Arbeit betrachten. Insbesondere konzentrieren wir uns auf invertierte Spin-Ensembles, welche in der Regel instabile Systeme darstellen und ihre gespeicherte Energie an den Resonator abgeben. Die Stabilisierung eines solchen invertierten Spin-Ensembles ermöglicht eine Vielzahl praktischer Anwendungen in der modernen Quanteninformationstechnologie und reichen von Quantenspeichern und Quantenbatterien bis hin zu hochempfindlichen Photodetektoren.

In dieser Arbeit untersuchen wir verschiedene Stabilisierungsmechanismen für invertierte Spin-Ensembles, welche an eine einzelne Mode im Resonator gekoppelt sind. Zunächst stellen wir eine Methode der statischen Stabilisierung vor, die auf der inhomogenen Verbreiterung und der kollektiven Kooperativität des Ensembles beruht. Hier stellen wir einen allgemeinen Rahmen vor, der es uns ermöglicht, ein Kriterium für die Stabilität des invertierten Spin-Ensembles zu bestimmen.

Anschließend erweitern wir diese Methode auf periodisch modulierte Systeme, indem wir die Floquet-Theorie anwenden, die es uns wiederum ermöglicht, mit Hilfe des Propagators über eine Periode der Modulation eine Stabilitätsbedingung zu bestimmen. Während unser abgeleiteter Formalismus sehr allgemein ist, testen wir unsere Stabilisierungsmethode indem wir die Dynamik einer konkreten physikalischen Realisierung, basierend auf Stickstoff-Vakanzzentren in Diamant, simulieren. Dabei untersuchen wir auch den Effekt eines externen Probepulses, der auf ein stabilisiertes Spinsystem angewendet wird. Schließlich untersuchen wir den Stabilisierungsmechanismus im Detail und zeigen einen Zusammenhang zwischen der Stabilisierung und den Phasen des Resonatorfeldes und der Spins auf.

Die approbierte gedruckte Originalversion dieser Diplomarbeit ist an der TU Wien Bibliothek verfügbar
The approved original version of this thesis is available in print at TU Wien Bibliothek.

Die approbierte gedruckte Originalversion dieser Diplomarbeit ist an der TU Wien Bibliothek verfügbar
The approved original version of this thesis is available in print at TU Wien Bibliothek.

Contents

1. Introduction **2**

2. Theoretical Background **4**
2.1. Cavity QED 4
2.2. Tavis-Cummings Hamiltonian 5
2.3. Maxwell-Bloch Equations 6
2.3.1. Linearization 8
2.4. Ensembles of Spins inside a Cavity 9
2.4.1. System Losses 9
2.4.2. Inhomogeneous Broadening 10
2.4.3. Cooperativity 11
2.4.4. Inverted Spin Ensemble 11
2.5. Numerical Solution of the Maxwell-Bloch Equations 11

3. Static Stabilization **13**
3.1. Dynamical Evolution of an Inverted Ensemble 13
3.2. Stabilization of an Inverted Ensemble 17
3.3. External Pulse 20
3.3.1. External Pulse without Stabilization 21
3.3.2. External Pulse with Stabilization 23

4. Dynamic Stabilization using Floquet Engineering **25**
4.1. Floquet Theory 25
4.1.1. One-period Propagator 26
4.2. Single Spin System 28
4.2.1. Parameter Scan 28
4.2.2. Stabilization Mechanism 30
4.3. Spin Ensemble 33
4.3.1. External Pulse 35

5. Summary and Outlook **40**

A. Deriving the Maxwell-Bloch Equations **42**

Acknowledgments **47**

Die approbierte gedruckte Originalversion dieser Diplomarbeit ist an der TU Wien Bibliothek verfügbar
The approved original version of this thesis is available in print at TU Wien Bibliothek.

Chapter 1.

Introduction

The field of cavity quantum electrodynamics (QED) is concerned with the interaction between matter and the quantized field modes inside a resonator. Cavity QED was already initiated in the 1940s by the pioneering work of Purcell [1] and became a fast-growing field of research that enabled tests of fundamental physics and the spectacular realization of thought experiments with single photons and atoms [2]. The latter development finally also lead to the Nobel Price in Physics in 2012 [3, 4].

By restricting the free electromagnetic field to only selected quantized field modes, as is the case for cavity QED, the theoretical description is significantly simplified and thus makes it more accessible both for theoretical and experimental studies. The first fully quantum description of an atom coupled to a single mode of the quantized field inside a resonator was presented in 1963 by Jaynes and Cummings [5]. This exactly solvable model now serves as a basis for the understanding of numerous quantum optics phenomena, e.g., vacuum-field Rabi oscillations and the collapse and revival of atomic oscillations [6, 7]. Since then, cavity QED paved the way for many technological applications [8–10], especially concerning quantum information processing [11–13] in hybrid quantum systems [14, 15].

In this thesis, we consider an ensemble of two-level systems strongly coupled to a single cavity mode [16, 17]. Here, the coupling strength between the atoms and the field mode exceeds the total losses of the system, allowing for coherent, self-induced oscillations in the atomic excitations, known as quantum Rabi oscillations [18–20] and a splitting of the cavity transmission spectrum into two resolvable peaks—an effect known as Rabi splitting [21]. Physical realizations of such strongly coupled systems include single molecules in plasmonic nanocavities [22, 23], artificial atoms based on superconducting qubits [24, 25] and quantum dots [26], as well as solid-state spin ensembles [27–32]. While the formalism presented in this thesis is very general, we assume for our calculations a specific realization of a spin-cavity system based on negatively charged nitrogen-vacancy (NV) defects in a diamond crystal [27–32].

Quite recently, ensemble-based systems gained interest in the field of quantum batteries [33, 34]. Here, energy is stored in the inverted spin system and then discharged in a controllable manner. Such excited-state ensembles have been stud-

Die approbierte gedruckte Originalversion dieser Diplomarbeit ist an der TU Wien Bibliothek verfügbar
The approved original version of this thesis is available in print at TU Wien Bibliothek.
TU Bibliothek Your knowledge hub WIEN

ied extensively within the field of superradiance [35], ranging from fundamental studies of the superradiant emission [36] to technological applications within laser physics [37]. A great challenge in this application lies in the stabilization of the inverted spin ensembles. In the context of the quantum battery, this is analogous to keeping it well isolated from its environment so it holds its energy for a sufficiently long time. A discharging of the battery can be triggered either by disabling the stabilization mechanism or by an external pulse, which is able to overcome the stabilization mechanism. Such a setup could thus also be used as a photo-detector for weak photonic pulses. However, this enforces two constraints on the stabilization mechanism: it should be strong enough to keep the ensemble in its inverted state, preventing a spontaneous release of the stored energy, while still allowing such a decay to be triggered by a (weak) external pulse.

In this thesis we study two different stabilization mechanisms: static stabilization based on the inhomogeneous broadening of the spin ensemble as introduced by Julsgaard and Mølmer [38] and dynamic stabilization based on periodic modulation of the spin detuning. These methods are investigated here both purely theoretically and through numerical simulations of the system's time evolution.

This thesis is structured as follows: first we introduce the theoretical framework, which the main results of this thesis are based on. The framework mainly consists of a Lindblad Master equation approach to derive the semi-classical equations of motion in the form of Maxwell-Bloch equations, which can be solved numerically. We then demonstrate a static stabilization method and derive a condition for stability, which is equivalent to the condition presented by Julsgaard and Mølmer in Ref. [38]. Then we show a new method of stabilization, based on a periodic modulation of the system. For this, we briefly introduce the concept of Floquet theory, which allows us to extend our condition for stability to time-periodic systems. We proceed to demonstrate the resulting system dynamics and also show the effect of an external pulse on a stabilized inverted spin ensemble. Finally, a summary of the main results is given with an outlook for future investigations.

Die approbierte gedruckte Originalversion dieser Diplomarbeit ist an der TU Wien Bibliothek verfügbar
The approved original version of this thesis is available in print at TU Wien Bibliothek.
TU Bibliothek Your knowledge hub WIEN

Chapter 2.

Theoretical Background

2.1. Cavity QED

The interaction of light and matter inside a cavity is thoroughly described in the field of cavity quantum electrodynamics. Here, the word *cavity* refers to a resonator for electromagnetic radiation, and the matter inside the cavity is described in the following as a collection of two-level systems (TLS). Starting from Maxwell's equations, one can derive a formalism treating the modes of the electromagnetic field as harmonic oscillators, which after quantization can be treated as quantum harmonic oscillators. Limiting the number of electromagnetic modes through the resonator drastically simplifies the theoretical description of cavity QED compared to conventional QED in free space. The first quantum mechanical treatment of a TLS inside a cavity was presented by Jaynes and Cummings who introduced an exactly solvable model for a TLS interacting with a single cavity mode [5]. For a comprehensive introduction of the quantum mechanical description of a field inside a cavity, the reader is referred to one the following excellent textbooks [2, 39, 40].

A paradigm example of cavity QED setups are nitrogen-vacancy (NV) centers inside diamond [27–32]. This point-like defect in a diamond lattice results in an energy level structure, which features an electron spin triplet ($S = 1$) as its (optical) ground state [41]. Due to inherent dipole-dipole interactions, this paramagnetic ground state shows a zero field splitting in the microwave regime, where the states $m_s = \pm 1$ and $m_s = 0$ are separated by $\sim 2.88\,\mathrm{GHz}$ [42]. This ground state splitting can be further Zeeman-tuned, forming a tunable TLS, which can be coupled to a superconducting microwave resonator. In order to coherently exchange quantum information between such a spin and the cavity, these two system constituents are required to be strongly coupled to each other. This can be achieved by collectively coupling the cavity to a large ensemble of spins. However, this comes with the challenge of having to deal with the inhomogeneous broadening in the spin transition frequencies, which is explained in more detail in Subsection 2.4.2.

The quantum description of such a spin-cavity system is given in terms creation and annihilation operators $(\hat{a}^\dagger, \hat{a})$ for the photons inside the cavity, which satisfy

Die approbierte gedruckte Originalversion dieser Diplomarbeit ist an der TU Wien Bibliothek verfügbar
The approved original version of this thesis is available in print at TU Wien Bibliothek.

the bosonic commutation relation

$$\left[a, a^\dagger\right] = 1, \tag{2.1}$$

as well as excitation and de-excitation operators $(\hat{\sigma}_k^+, \hat{\sigma}_k^-)$ for the individual TLSs, satisfying

$$\left[\sigma_k^+, \sigma_j^-\right] = \sigma_k^z \delta_{kj} \quad \text{and} \quad \left[\sigma_k^z, \sigma_j^\pm\right] = \pm 2\sigma_k^\pm \delta_{kj}\,. \tag{2.2}$$

Note that the spin excitation and de-excitation operators are related to the Pauli operators σ^x and σ^y by

$$\sigma_k^+ = \frac{1}{2}\left(\sigma_k^x + i\sigma_k^y\right) \quad \text{and} \quad \sigma_k^- = \frac{1}{2}\left(\sigma_k^x - i\sigma_k^y\right). \tag{2.3}$$

Using these operators, the interaction between a single cavity mode and an ensemble of spins can be described by the Tavis-Cummings Hamiltonian.

2.2. Tavis-Cummings Hamiltonian

The Tavis-Cummings Hamiltonian [43] extends the Jaynes-Cummings model, which concerns a single TLS inside a cavity, to a system of many spins. In the rotating-wave approximation (RWA), where the counter-rotating terms $\sigma_k^- a$ and $\sigma_k^+ a^\dagger$ are neglected, the Hamiltonian is given by ($\hbar = 1$)

$$H = \omega_c a^\dagger a + \frac{1}{2}\sum_{k=1}^{N} \omega_k \sigma_k^z + \sum_{k=1}^{N}\left(g_k \sigma_k^- a^\dagger + g_k^* \sigma_k^+ a\right) + i\left[\eta(t) a^\dagger e^{-i\omega_p t} - \eta(t)^* a e^{i\omega_p t}\right]. \tag{2.4}$$

The first term in Eq. (2.4) corresponds to the energy of the free cavity field with frequency ω_c, while second term describes the energy of the individual spins with frequencies ω_k. The third term represents the Jaynes-Cummings type interaction between the spins and the cavity mode with coupling strengths g_k. Since the phase of the coupling strength is physically not important, we can choose g_k either real or imaginary. In this thesis we choose g_k to be real $g_k = g_k^*$. The last term in Eq. (2.4) corresponds to an external driving field with frequency ω_p and amplitude $\eta(t)$ injected into the cavity. For convenience, we again choose $\eta(t)$ to be real-valued.

The Tavis-Cummings Hamiltonian without external driving belongs to the class of exactly solvable Richardson-Gaudin models [44] and can in principle be solved via a Bethe ansatz technique [45–47]. However, since we are dealing with realistic open systems in this thesis, we will focus on the driven and dissipative dynamics of the spin-cavity system. Thus, we present below the corresponding master equation approach and the resulting equations of motion for the expectation values.

Die approbierte gedruckte Originalversion dieser Diplomarbeit ist an der TU Wien Bibliothek verfügbar
The approved original version of this thesis is available in print at TU Wien Bibliothek.
TU Bibliothek Your knowledge hub WIEN

2.3. Maxwell-Bloch Equations

A general solution for the Tavis-Cummings model in an open dissipative system can be obtained by the Lindblad master equation approach [48, 49]. This approach is based on the fundamental Born-Markov approximation which assumes that the combined density matrix of the system and the environment can be factorized as $\rho_{\text{tot}}(t) = \rho(t) \otimes \rho_{\text{env}}(0)$, such that the state of the large environment $\rho_{\text{env}}(0)$ is not affected by the evolution of $\rho(t)$. Additionally, we attribute to the environment a very short memory time, such that correlations between operators of the environment decay fast compared to the intrinsic time scale of the spin-cavity system. This approximation is typically well satisfied for spin-cavity systems. A derivation of the Lindblad master equation can be found in numerous textbooks [48–50] and yields the equation

$$\frac{d}{dt}\rho(t) = \mathcal{L}[\rho] = -i[H, \rho] + \mathcal{L}_D[\rho], \tag{2.5}$$

where $\rho(t)$ is the aforementioned density matrix of the system. The losses which are due to the coupling of the spin-cavity system to the surrounding environment are contained in the Lindblad term $\mathcal{L}_D$ given by

$$\begin{aligned}\mathcal{L}_D[\rho] =& \kappa \left(2a\rho a^\dagger - a^\dagger a\rho - \rho a^\dagger a\right) + \gamma_h \sum_{k=1}^{N} \left(2\sigma_k^- \rho \sigma_k^+ - \sigma_k^+ \sigma_k^- \rho - \rho \sigma_k^+ \sigma_k^-\right) \\ &+ \gamma_p \sum_{k=1}^{N} \left(\sigma_k^z \rho \sigma_k^z - \rho\right).\end{aligned} \tag{2.6}$$

This term accounts for three different types of dissipative mechanisms. The first term in Eq. (2.6) corresponds to cavity losses with rate κ. The second term accounts for the radiative decay of the individual spins with rate γ_h and the last term gives the non-radiative dephasing with rate $\gamma_p/2$. We note here that the radiative and non-radiative decay rates can be related to the more commonly known longitudinal and transverse relaxation times T_1 and T_2 as will be explained in Subsection 2.4.1. In addition, it should also be noted that we neglect thermal excitations in Eq. (2.6) (i.e $k_B T \ll \hbar\omega_c, \hbar\omega_k$). A schematic of the system under investigation with all dissipative mechanisms can be seen in Figure 2.1.

In order to solve Eq. (2.5) in a system where the number of spins is of the order of 10^{10}, we have to take an approach to directly solve for the operator expectation values [51–54]. The resulting equation of motion for some operator O is obtained by multiplying O with the quantum master equation (2.5) and taking the trace, leading to

$$\frac{d}{dt}\langle O\rangle = \text{Tr}\left(-i\left[O, H\right]\rho + O\mathcal{L}_D[\rho]\right). \tag{2.7}$$

Together with a rotating frame transformation of the Tavis-Cummings Hamiltonian, one can calculate the corresponding expectation values for the operators a, σ_k^-, and

Die approbierte gedruckte Originalversion dieser Diplomarbeit ist an der TU Wien Bibliothek verfügbar
The approved original version of this thesis is available in print at TU Wien Bibliothek.
TU Bibliothek Your knowledge hub WIEN

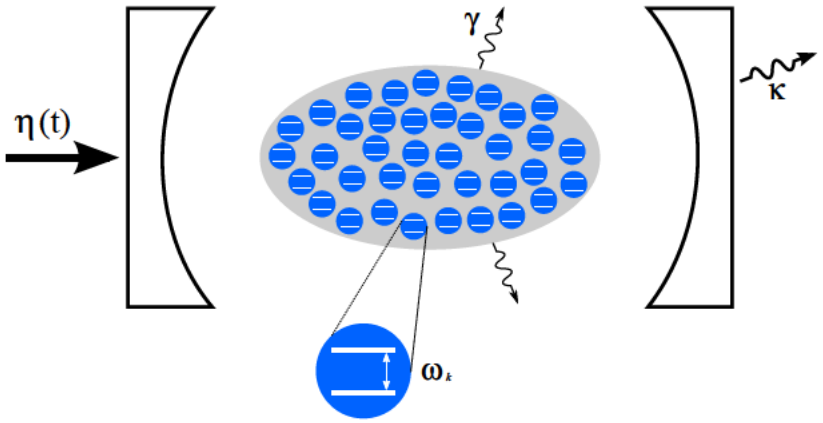

Figure 2.1. Schematic of the physical system under investigation. An ensemble of two-level systems (blue) with transition frequencies ω_k is placed inside a cavity and tuned to the resonance frequency ω_c. An external field $\eta(t)$ can be applied to interact with the ensemble. System losses, due to the coupling to the surrounding environment, are described by individual spin decay with rates γ_h, γ_p and the cavity dissipation with rate κ.

σ_k^z (a detailed derivation can be seen in Appendix A). This results in the following set of equations:

$$\frac{d}{dt}\langle a\rangle = -\left(\kappa + i\Delta_c\right)\langle a\rangle - i\sum_{k=1}^{N} g_k\langle\sigma_k^-\rangle + \eta(t), \tag{2.8}$$

$$\frac{d}{dt}\langle\sigma_k^-\rangle = -\left(\gamma_h + 2\gamma_p + i\Delta_k\right)\langle\sigma_k^-\rangle + ig_k\langle\sigma_k^z a\rangle, \tag{2.9}$$

$$\frac{d}{dt}\langle\sigma_k^z\rangle = -2\gamma_h\left(\langle\sigma_k^z\rangle + 1\right) - 4g_k\,\mathrm{Im}\left(\langle\sigma_k^- a^\dagger\rangle\right), \tag{2.10}$$

with $\Delta_c = \omega_c - \omega_p$ and $\Delta_k = \omega_k - \omega_p$. We note that this set of differential equations is not closed, since the expectation values for $\langle\sigma_k^-\rangle$ and $\langle\sigma_k^z\rangle$ in Eq. (2.9) and Eq. (2.10) depend on the expectation values of $\langle\sigma_k^z a\rangle$ and $\langle\sigma_k^- a^\dagger\rangle$, which in turn depend on the expectation value of the product of three operators. This corresponds to the Bogoliubov-Born-Green-Kirkwood-Yvon (BBGKY) hierarchy [55], where for a system of interacting particles, the dynamic of an expectation value involving n operators depends on expectation values involving $n+1$ operators. While there have been several approaches presented to truncate this infinite set of equations (see e.g. [31, 52, 56–58]), in this thesis, we use the self-consistent field approximation [56], which consists in factorizing the operator expectation values containing field and spin operators, e.g., by

$$\langle\sigma_k^z a\rangle \approx \langle\sigma_k^z\rangle\langle a\rangle. \tag{2.11}$$

This factorization of expectation values is well justified in the limit of large spin

Die approbierte gedruckte Originalversion dieser Diplomarbeit ist an der TU Wien Bibliothek verfügbar
The approved original version of this thesis is available in print at TU Wien Bibliothek.

ensembles ($\sim 10^{10}$), where correlations between the cavity field and individual spins become negligible [49, 59]. For a system of N spins, this leads to a closed set of $2N + 1$ equations:

$$\frac{d}{dt}\langle a\rangle = -\left(\kappa + i\Delta_c\right)\langle a\rangle - i\sum_{k=1}^{N} g_k\langle\sigma_k^-\rangle + \eta(t), \tag{2.12}$$

$$\frac{d}{dt}\langle\sigma_k^-\rangle = -\left(\gamma_\perp + i\Delta_k\right)\langle\sigma_k^-\rangle + ig_k\langle\sigma_k^z\rangle\langle a\rangle, \tag{2.13}$$

$$\frac{d}{dt}\langle\sigma_k^z\rangle = -\gamma_\parallel\left(\langle\sigma_k^z\rangle + 1\right) - 4g_k\,\mathrm{Im}\left(\langle\sigma_k^-\rangle\langle a^\dagger\rangle\right), \tag{2.14}$$

where we also introduced for convenience the decay rates $\gamma_\parallel \equiv 2\gamma_h$ and $\gamma_\perp \equiv \gamma_h + 2\gamma_p$. These equations are equivalent to the seminal Maxwell-Bloch equations which form an integral basis for the description of semiclassical quantum optics phenomena [55].

2.3.1. Linearization

While the Maxwell-Bloch equations allow us to analyze the complete, nonlinear dynamics for large spins ensembles involving many excitations, it is often useful to linearize the equations similar to a Holstein-Primakoff approximation [60], which can be applied in the limit where only a few spins in the ensemble get excited. In this approximation, the number of spin excitations are assumed to remain almost constant during the simulation period. This allows us to fix the value of $\langle\sigma_k^z\rangle = \zeta = \text{const}$ and to linearize the Maxwell-Bloch equations:

$$\frac{d}{dt}\langle a\rangle = -\left(\kappa + i\Delta_c\right)\langle a\rangle - i\sum_{k=1}^{N} g_k\langle\sigma_k^-\rangle + \eta, \tag{2.15}$$

$$\frac{d}{dt}\langle\sigma_k^-\rangle = -\left(\gamma_\perp + i\Delta_k\right)\langle\sigma_k^-\rangle + i\zeta g_k\langle a\rangle. \tag{2.16}$$

This approximation only remains valid for a small external drive η, as this directly impacts excitations of the ensemble. Additionally, we have to assume that non-radiative processes constitute the dominant dephasing mechanism, i.e. $\gamma_h \ll \gamma_p$ and therefore

$$\gamma_\parallel \ll \gamma_\perp. \tag{2.17}$$

Moreover, the cavity decay rate κ has to be orders of magnitude larger than the longitudinal relaxation rate $\gamma_\perp$ and thus holds

$$\gamma_\parallel \ll \kappa. \tag{2.18}$$

This ensures that the change in $\langle\sigma_k^z\rangle$ is small and we can fix it at a constant value. The two inequalities (2.17) and (2.18) are usually very well fulfilled, for the setup of nitrogen-vacancy centers considered in this thesis [30, 61].

Die approbierte gedruckte Originalversion dieser Diplomarbeit ist an der TU Wien Bibliothek verfügbar
The approved original version of this thesis is available in print at TU Wien Bibliothek.
TU Bibliothek Your knowledge hub WIEN

This linearization is crucial when trying to analyze the stability of a spin ensemble with regards to small perturbations and will be used to derive the regions of stability in the following chapters. Note that for the special case of $\zeta = -1$ this becomes the conventional Holstein-Primakoff approximation.

2.4. Ensembles of Spins inside a Cavity

The spin ensemble, described by the Maxwell-Bloch equations, contains many interesting features, such as cooperative effects (e.g. superradiance [35]) that we will focus our attention on in the following.

2.4.1. System Losses

As mentioned in Section 2.3, the individual spin decay is described by the relaxation rates γ_h and γ_p in the Lindbladian Eq. (2.6), which correspond to the commonly used T_1 and T_2 relaxation times via the relation

$$T_1 = \frac{1}{2\gamma_h} \quad \text{and} \quad T_2 = \frac{1}{\gamma_h + 2\gamma_p}. \tag{2.19}$$

The T_1 relaxation describes the longitudinal decay, where the spins relax towards their ground state, given by $\langle \sigma_k^z \rangle = -1$. This decay can occur either through phonon mediated processes [62] or through spontaneous emission. The T_2 relaxation corresponds to a dephasing of the spins along the z-axis. These two different relaxation mechanisms are shown in Figure 2.2.

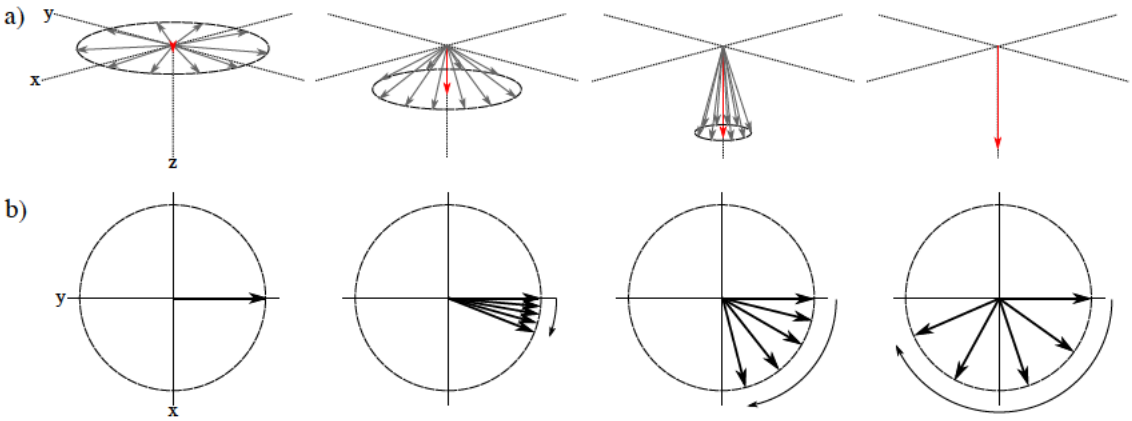

Figure 2.2. Graphical description of the T_1 (panel a) and T_2 (panel b) relaxation mechanism for a small number of spins. In T_1 relaxation the ensemble expectation value of σ_z (marked in red) tends towards the ground state, while in T_2 relaxation the spins dephase along the z-axis.

Die approbierte gedruckte Originalversion dieser Diplomarbeit ist an der TU Wien Bibliothek verfügbar
The approved original version of this thesis is available in print at TU Wien Bibliothek.

Photon losses are described by the parameter κ as the cavity dissipation rate, also referred to as cavity line width. Note, that in this case κ describes the half-width-at-half-maximum (HWHM) of the line width. Together with the central operating frequency, this parameter gives rise to the quality of the cavity $Q = \omega_c/\kappa$, which describes how under-damped or over-damped the resonator is. In other words, it describes how much energy is stored compared to the energy dissipated.

2.4.2. Inhomogeneous Broadening

The coupling strength of the spins to the cavity and the transition frequencies are described by the parameters g_k and ω_k, respectively. Naturally, the individual spins in an ensemble have slightly different local environments leading to differences in both their transition frequencies and coupling strengths. This inhomogeneous broadening leads to several interesting effects and usually acts as the main source for dephasing in the spin ensemble [30, 31]. As a result, the coherence time can be drastically decreased, restricting the performance in processing and storing quantum information [63–65]. An accurate modeling of the inhomogeneous broadening is thus essential for describing and understanding many quantum phenomena.

While both coupling strengths g_k and transitions frequencies ω_k can exhibit different distributions, they are often combined in a continuous spectral spin distribution [31]

$$\rho(\omega) \equiv \sum_{k=1}^{N} \frac{g_k^2 \delta(\omega - \omega_k)}{\Omega^2}, \tag{2.20}$$

where $\Omega^2 = \sum_{k=1}^{N} g_k^2$ is the collective coupling strength. This spectral spin distribution can be determined from transmission measurements in the weak excitation regime [29].

In the highly nonlinear regime of the Maxwell-Bloch equations, the different distributions of the coupling strength and spin transition frequencies become more relevant. In principle, they can be incorporated separately, by two different distributions. However, this makes the situation more complicated, since in the case that the individual distributions are unknown, additional assumptions have to be made.

Moreover, note that for a fixed spectral spin distribution $\rho(\omega)$, the Maxwell-Bloch equations show an invariance under changes in the number of spins N, using the following transformation

$$g_k \to g_k/\sqrt{N}, \quad \langle a \rangle \to \langle a \rangle/\sqrt{N}, \quad \eta \to \eta/\sqrt{N}. \tag{2.21}$$

This can be used to reduce the number of spins in the numerical calculations.

Die approbierte gedruckte Originalversion dieser Diplomarbeit ist an der TU Wien Bibliothek verfügbar
The approved original version of this thesis is available in print at TU Wien Bibliothek.
TU Bibliothek Your knowledge hub WIEN

2.4.3. Cooperativity

The cooperativity C_k, defined as

$$C_k \equiv \frac{g_k^2}{\gamma_\perp \kappa (1 + \Delta_k^2/\gamma_\perp^2)}. \tag{2.22}$$

is a dimensionless parameter, used to describe the ratio of the coupling strength of the spins to the decay rates of the system. The collective system cooperativity C is then simply defined as the sum of the individual spin cooperativities

$$C \equiv \sum_{k=1}^{N} C_k. \tag{2.23}$$

When operating a cavity in the strong-coupling regime, one can usually assume that $C \gg 1$, since this yields a necessary condition for strong-coupling effects, like vacuum Rabi oscillations, to occur.

2.4.4. Inverted Spin Ensemble

In the following chapters we will investigate the behavior of inverted or partially inverted spin ensembles. We refer to a spin ensemble as completely inverted, when all involved spins are excited, such that $\langle \sigma_k^z \rangle = 1$ for all k. In this case the energy stored in the spin ensemble is at its maximum. However, since fully inverted spin ensembles are experimentally hard to accomplish, we also consider partially inverted ensembles, where the spins are excited only to some extent $\langle \sigma_k^z \rangle = \zeta$, $\zeta > -1$.

The inversion renders the spin ensemble inherently unstable, as it will always tend towards its ground state $\langle \sigma_k^z \rangle = -1$ (note that $k_B T \ll \omega_k$) through individual spin decay and energy losses by the cavity dissipation rate.

While the system losses describe the coupling of the system to the environment, the inhomogeneous broadening, cooperativity and inversion present important internal system quantities. Together, this set of parameters forms the basis for describing the relevant dynamical processes of spin ensembles in a cavity.

2.5. Numerical Solution of the Maxwell-Bloch Equations

The Maxwell-Bloch equations form a set of $2N + 1$ complex, non-linear, first order differential equations, which can in principle be solved for given initial conditions, e.g., using a standard Runge-Kutta method [66]. However, in order to enter the strong coupling regime, the necessary number of spins N lies somewhere in the range of $\sim 10^{10}$. To make the problem numerically tractable, we have to first

Die approbierte gedruckte Originalversion dieser Diplomarbeit ist an der TU Wien Bibliothek verfügbar
The approved original version of this thesis is available in print at TU Wien Bibliothek.

divide the spin ensemble into L equally sized frequency intervals $\delta\omega$ with $L \ll N$. Each interval, denoted by the Greek index μ is assumed to contain M_μ spins with similar coupling strengths g_μ and transition frequencies ω_μ. Using these frequency bins, we can proceed in two different ways:

1. **Inhomogeneous coupling.** Here we assume that each frequency bin effectively represents one "large" spin with coupling strength g_μ and transition frequency ω_μ. The corresponding coupling strength can then be determined from the spectral spin distribution $\rho(\omega)$ by the inverse transformation $g_\mu = \Omega[\rho(\omega_\mu)/\sum_{\nu=1}^{L}\rho(\omega_\nu)]^{1/2}$. This way, we can drastically reduce the number of equations to $2L+1$, which can be solved numerically.

2. **Inhomogeneous cluster size.** Different to the inhomogeneous coupling distribution, we assume here, that each frequency bin is occupied by a different number of spins M_μ. All spins are then assumed to couple with the same coupling strength $g_k = g_0 = \Omega/\sqrt{N}$, while the number of spins in each frequency bin follows the spectral spin distribution $M_\mu = N\rho(\omega_\mu)/\sum_{\nu=1}^{L}\rho(\omega_\nu)$.

If not stated otherwise, we use the inhomogeneous coupling in the following sections, as it allows us to explicitly write down the system Jacobi matrix, which is needed to derive the regions of stability for the ensemble.

The number of clusters has to be chosen such that the spectral spin distribution can be properly represented. Too few frequency clusters lead to artifacts in the simulation due to the frequency discretization. To ensure that no such artifacts occur, the frequency spacing of adjacent clusters has to be chosen such that the factor $1/|\omega_\mu - \omega_{\mu+1}|$ is larger than the covered time of the system's evolution.

While our formalism is very general, we will consider a concrete physical realization based on nitrogen-vacancy centers in diamond in this thesis [27–32]. This allows us to use parameters obtained from physical experiments and also compare the results to possible experiments. Thus, we model the spectral spin distribution as a q-Gaussian distribution $\rho(\omega)$ [67, 68], given by

$$\rho(\omega) = D\left[1-(1-q)\,(\omega-\omega_s)^2/\Delta^2\right]^{1/(1-q)}, \tag{2.24}$$

where q is dimensionless shape parameter, $\gamma_{inh} = 2\Delta\sqrt{(2^q-2)/(2q-2)}$ is the full width at half maximum (FWHM), and D is a normalization constant. From transmission experiments on NV-centers, the shape parameter can be estimated as $q = 1.39$ [29].

Die approbierte gedruckte Originalversion dieser Diplomarbeit ist an der TU Wien Bibliothek verfügbar
The approved original version of this thesis is available in print at TU Wien Bibliothek.

Chapter 3.

Static Stabilization

In this chapter we investigate the effect of different static stabilization mechanisms. We start by showing the dynamic evolution of an inverted spin ensemble, without any stabilization mechanisms. Here we introduce the relevant dynamical variables we use to characterize the ensemble's dynamics. Then we derive a condition for stability under the Holstein-Primakoff approximation using the system's Jacobi matrix and show that this ansatz equivalently yields the criterion obtained by Julsgaard and Mølmer [38]. We subsequently apply this method and present different examples of stabilized ensembles. Finally we show, that the stored energy in such a stabilized ensemble can be extracted through an external pulse acting on the cavity.

3.1. Dynamical Evolution of an Inverted Ensemble

The dynamical evolution of an inverted spin ensemble is determined by the Maxwell-Bloch Eqs. (2.12)-(2.14), presented in Section 2.3. In order to visualize the system's dynamics, we introduce mean values for the total spin orientation, effectively describing a single "giant" spin. For a frequency discretization using inhomogeneous cluster sizes (see Section 2.5) the ensemble mean, denoted by the missing subscript index, is then given by

$$\langle \bar{\sigma}^i \rangle = \frac{1}{N} \sum_{\mu=1}^{L} M_\mu \langle \sigma_\mu^i \rangle, \tag{3.1}$$

with i representing one of x, y, or z. Note that the individual spin orientations can be extracted from the observables $\langle \sigma_k^+ \rangle$ and $\langle \sigma_k^z \rangle$ using the relations

$$\langle \sigma_k^x \rangle = 2\,\mathrm{Re}\langle \sigma_k^+ \rangle \quad \text{and} \quad \langle \sigma_k^y \rangle = 2\,\mathrm{Im}\langle \sigma_k^+ \rangle. \tag{3.2}$$

We will further refer to this averaged spin direction as the "global" spin.

As initial condition, we assume a partially inverted spin ensemble, such that $\langle \sigma_k^z \rangle (t = 0) = \zeta$. This corresponds to a spin with a global tipping angle $\theta = \arccos(\zeta)$ from the z-axis in the Bloch sphere. For convenience, the azimuthal angle ϕ is chosen to be 0. This initial tipping angle is necessary to initiate a decay

Die approbierte gedruckte Originalversion dieser Diplomarbeit ist an der TU Wien Bibliothek verfügbar
The approved original version of this thesis is available in print at TU Wien Bibliothek.

of the ensemble as described below. Additionally, we assume that there are initially no photons in the cavity, meaning that $\langle a \rangle (t = 0) = 0$.

Next, the dynamical evolution of this spin ensemble, operating at the central cavity frequency ($\Delta_c = 0$) and with no external drive ($\eta = 0$), is simulated by numerically integrating the Maxwell-Bloch equations. The parameters of the simulation are determined to resemble the behavior of a spin ensemble given by an experimental realization using NV centers in diamond [27–32]. The total coupling strength is chosen as $\Omega/2\pi = \sqrt{\sum_{j=1}^{N} g_j^2}/2\pi = 4.745$ MHz, $\gamma_{inh}/2\pi = 7.182$ MHz, $\gamma_{\parallel}/2\pi = 100$ Hz, $\gamma_{\perp}/2\pi = 125$ kHz and $\kappa/2\pi = 0.695$ MHz. For the simulation we choose an ensemble of $N = 10^{12}$ spins clustered into frequency $L = 1000$ bins. If not stated otherwise, these parameters are used in all following simulations. The results for the absolute value $|\langle a \rangle|^2$ of the cavity amplitude and the three spatial components $\langle \bar{\sigma}^i \rangle$ of the global spin vector are depicted in Figure 3.1 for various values of the global tipping angle θ. The dynamics show an immediate decay of the

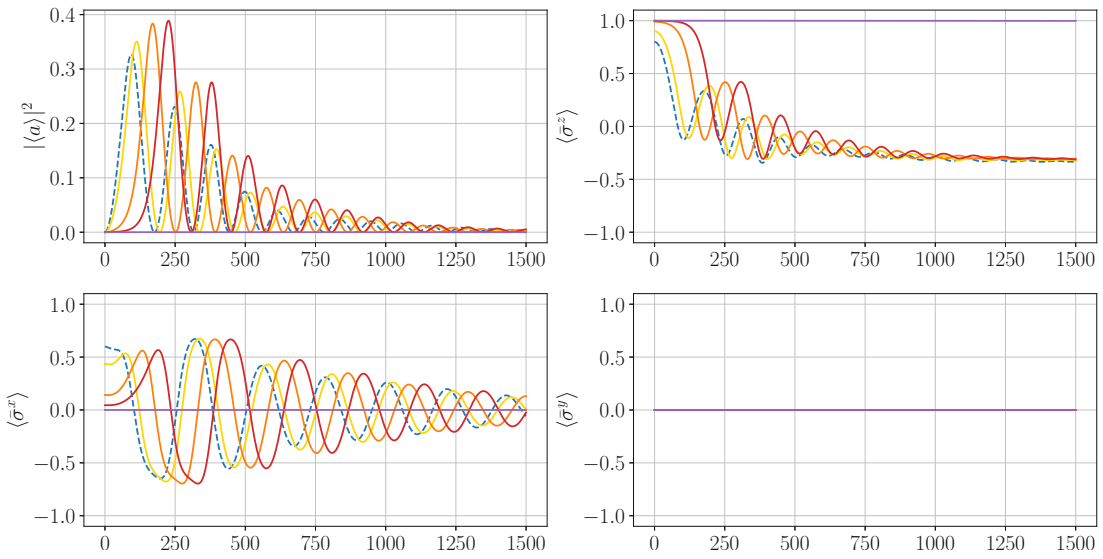

Figure 3.1. Dynamics of the absolute value $|\langle a \rangle|^2$ of the cavity amplitude and the three spatial components $\langle \bar{\sigma}^i \rangle$ of the global spin vector for a partially inverted ensemble with $\zeta = 0.8$ (blue dashed), 0.9 (gold), 0.99 (orange), 0.999 (red), 1 (purple). This corresponds to the tipping angles $\theta = 36.87°$, $25.85°$, $8.11°$, $2.56°$ and $0°$, respectively. The case $\zeta = 0.8$ is shown, since it resembles a level of inversion which can realistically be achieved in an experimental realization and will thus be used in most simulations throughout this thesis.

spin ensemble with concomitant Rabi oscillations, indicating that the system is in the strong coupling regime ($C \gg 1$) due to the strong coupling of the ensemble to

Die approbierte gedruckte Originalversion dieser Diplomarbeit ist an der TU Wien Bibliothek verfügbar
The approved original version of this thesis is available in print at TU Wien Bibliothek.

the cavity ($\Omega > \kappa, \gamma$) [28, 30]. Over the simulated time period, we only observe the fast decay related to the cavity dissipation and transversal spin relaxation ($\sim 1/\kappa$, T_2). The Rabi oscillations disappear on a time scale given by $1/\gamma_{inh}$ due to the dephasing caused by the inhomogeneous broadening of the spins. The system will finally settle into its ground state on a much longer time scale related to T_1.

Since in all of the above studied cases, the azimuthal angle in the initial spin condition was chosen to be $\phi = 0$, the global spin vector only oscillates in the x-z-plane of the Bloch sphere. This behavior can be clearly explained by examining the form of the Maxwell-Bloch equations.

As we observed in Figure 3.1 the collective decay of the spin ensemble into the cavity is triggered by a global tipping angle. If we choose $\zeta = 1$ such that the spins point exactly to the north pole of the Bloch sphere, the dynamics of the system is inhibited, with the spins decaying only individually at rate γ_h. Since γ_h is negligibly small in our simulations, the spin ensemble seems to remain in its inverted position, corresponding to an unstable fixed point. However, even the slightest deviation from the z-axis of the Bloch sphere, e.g. through a global tipping angle eventually leads to a collective and cavity-enhanced decay of the ensemble.

In the following, we present a procedure adapted from an experimental scheme developed in the group of Jörg Schmiedmayer to remove the global tipping angle by completely dephasing the spin ensemble. This detunes the spin ensemble from the cavity, which effectively decouples the spins from the resonator. As a result, the collective decay via the cavity is prohibited, while the spins dephase due to the inhomogeneous broadening, removing the global tipping angle as depicted schematically in Figure 3.2.

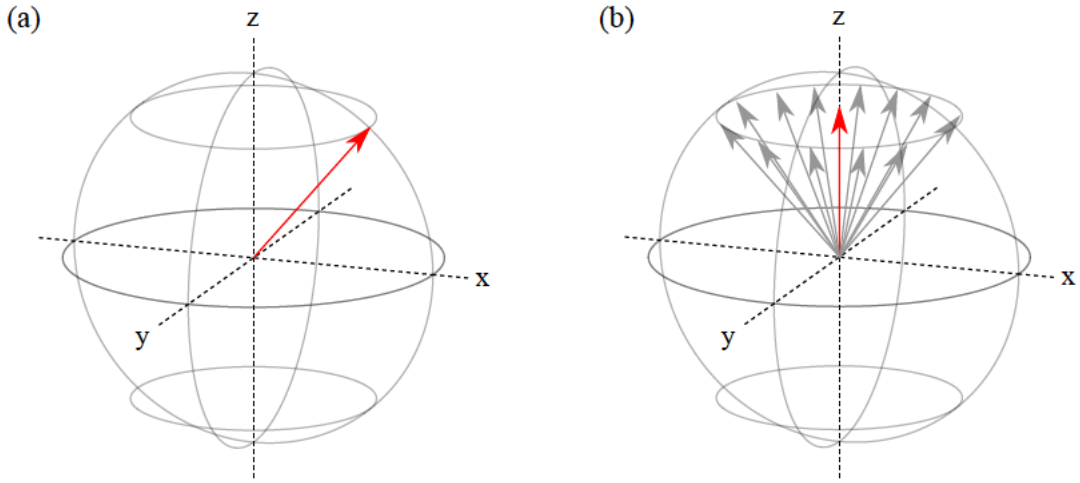

Figure 3.2. A global tipping angle is introduced in (a), where all spins are tipped by the same angle and in the same direction. (b) Due to the inhomogeneous broadening, the spins rotate around the z-axis of the Bloch sphere with different velocities and after some time they spread out equally, removing the global tipping angle.

Die approbierte gedruckte Originalversion dieser Diplomarbeit ist an der TU Wien Bibliothek verfügbar
The approved original version of this thesis is available in print at TU Wien Bibliothek.
TU Bibliothek Your knowledge hub WIEN

In the Maxwell-Bloch equations, a detuning of the spins is represented by an additional constant frequency offset ω_D in the spin transition frequencies:

$$\Delta_k = \omega_c - \omega_k \;\rightarrow\; \tilde{\Delta}_k = \omega_k + \omega_D - \omega_k. \tag{3.3}$$

The results of this dephasing mechanism can be seen in Figure 3.3 for different values of ω_D. For large detunings ($\omega_D > \gamma_{inh}$), the spins dephase faster than they can decay and the system can be fixed at its inverted position. If we choose ω_D large enough, the spins are effectively decoupled from the cavity. Although this stabilizes the ensemble in its inverted position, this also prevents the ability to store or extract any kind of information in the spin ensemble through the cavity.

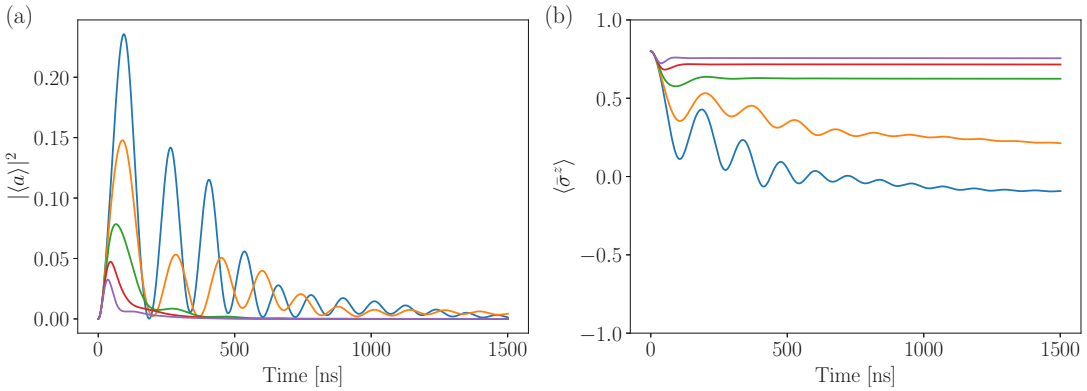

Figure 3.3. (a) The cavity field amplitude and (b) the ensemble mean $\langle \bar{\sigma}^z \rangle$ over time, with varying spin detuning ω_D. The initial condition is again chosen to be $\zeta = 0.8$ and a constant detuning ω_D is applied to the spin transition frequencies over the whole period of evolution with strengths $\omega_D = 5$ MHz (blue), 7.5 MHz (orange), 10 MHz (green), 12.5 MHz (red) and 15 MHz (purple).

After the global tipping angle is removed by keeping the spins detuned from the cavity for some time, we tune the spin ensemble back into resonance with the cavity. In Figure 3.4 (a,b), we present the corresponding dynamics of the cavity field $|\langle a \rangle|^2$ and the mean spin expectation value $\langle \bar{\sigma}^z \rangle$. Here, after a partial inversion of the spin ensemble with $\zeta = 0.8$, the spins are detuned by 15 MHz for 2000 ns (gray area in Figure 3.4). When the ensemble is finally brought back into resonance with the cavity at 2000 ns, we observe a decay after a few hundred nanoseconds. Although the global tipping angle is removed, the spins individually still have a tipping angle, which eventually triggers a collective and cavity-enhanced decay. Note, however, that this decay is delayed as compared to the case where a global tipping angle is present, as can be seen in Figure 3.4 (c,d). Therefore, the initial dephasing removes the global tipping angle and helps to delay the decay of the spin ensemble. This delay allows for interesting practical applications, as will be shown in Section 3.3

Die approbierte gedruckte Originalversion dieser Diplomarbeit ist an der TU Wien Bibliothek verfügbar
The approved original version of this thesis is available in print at TU Wien Bibliothek.
TU Bibliothek Your knowledge hub WIEN

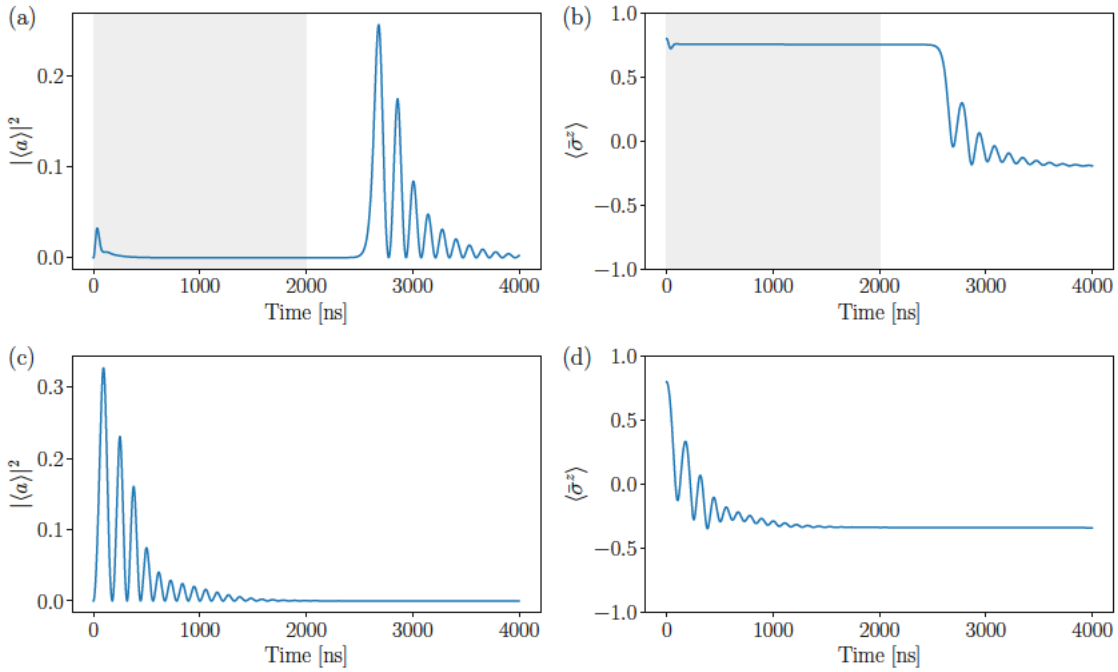

Figure 3.4. Panel (a,b): the spin ensemble with $\zeta = 0.8$ is initially detuned by 15 MHz from the central cavity for 2000 ns, in order to dephase the ensemble and to prevent a collective decay. After 2000 ns it is brought back into resonance with the cavity after which a self induced decay occurs with a short delay. For comparison, the same ensemble with no initial detuning is shown in panels (c) and (d), where an immediate decay can be observed.

3.2. Stabilization of an Inverted Ensemble

In a stable system, the spin ensemble does not collectively decay via the cavity and the spins remain inverted over a long period of time. Additionally, an external pulse still has to be able to interact with the spin ensemble through the cavity. In order to distinguish between stable and unstable systems, we first want to derive a stability criterion based on the system parameters. Therefore, we start with the approach suggested by Julsgaard and Mølmer [38], where they derived a stability criterion based on the cooperativity parameter C of the ensemble. It is found, that in order to achieve a stable system, C has to be decreased below a critical value, such that

$$C < 1. \tag{3.4}$$

Decreasing the system cooperativity is best achieved by increasing the cavity line width κ. Using the definition of the cooperativity in Eq. (2.23) one can express the

Die approbierte gedruckte Originalversion dieser Diplomarbeit ist an der TU Wien Bibliothek verfügbar
The approved original version of this thesis is available in print at TU Wien Bibliothek.

critical cavity line width for a stable ensemble as

$$\kappa_{crit} = \sum_{k=1}^{N} \frac{g_k^2}{\gamma_\perp(1 + \Delta_k^2/\gamma_\perp^2)}. \tag{3.5}$$

Any $\kappa \leq \kappa_{crit}$ renders the system unstable and leads to an eventual decay of the ensemble. This criterion, found in Ref. [38] can be easily adapted for partially inverted spin ensembles by multiplying the cooperativity with the inversion factor ζ, resulting in the condition

$$\zeta C < 1, \tag{3.6}$$

with the critical cavity line width

$$\kappa_{crit} = \zeta \sum_{k=1}^{N} \frac{g_k^2}{\gamma_\perp(1 + \Delta_k^2/\gamma_\perp^2)}. \tag{3.7}$$

When the cavity line width κ exceeds this critical value, the spins of the inhomogeneously broadened ensemble no longer decay cooperatively but remain inverted. To demonstrate this stabilization mechanism, we simulate the dynamical evolution of an inverted ensemble, which is initially dephased to remove the global tipping angle. The free evolution of the ensemble, after it is tuned back into resonance with the cavity is shown for varying values of κ in Figure 3.5. We notice, that as the cavity line width κ approaches κ_{crit}, the decay becomes smaller until we observe a stabilized system for values of κ close to κ_{crit}.

The transition from an unstable to a stable inverted spin ensemble can also be monitored by a stability analysis of the linearized system. For this purpose, we consider again an inverted spin ensemble with an inversion factor of ζ, a central spin frequency resonant with the cavity frequency, and no external drive. Under the assumption of a stable ensemble, the value of $\langle \sigma_k^z \rangle = \zeta$ can be fixed, which lets us linearize the Maxwell-Bloch equations to

$$\frac{d}{dt}\langle a \rangle = -\kappa \langle a \rangle - i \sum_{k=1}^{N} g_k \langle \sigma_k^- \rangle, \tag{3.8}$$

$$\frac{d}{dt}\langle \sigma_k^- \rangle = -\alpha_k \langle \sigma_k^- \rangle + i g_k \zeta \langle a \rangle, \tag{3.9}$$

where we introduced the shorthand notation $\alpha_k = \gamma_\perp + i\Delta_k$. This allows us to write the linear system in terms of a matrix differential equation and identify the

Die approbierte gedruckte Originalversion dieser Diplomarbeit ist an der TU Wien Bibliothek verfügbar
The approved original version of this thesis is available in print at TU Wien Bibliothek.
TU Bibliothek Your knowledge hub WIEN

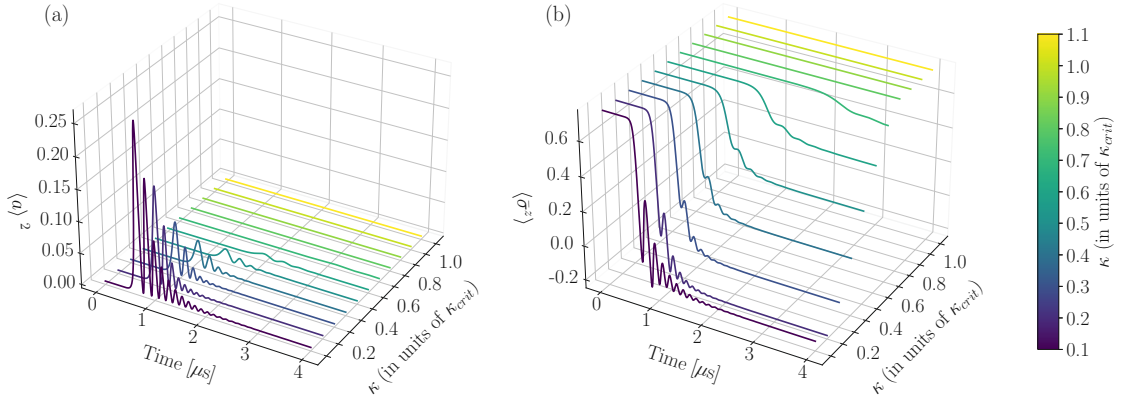

Figure 3.5. The effect of different values of κ on the free evolution of an inverted, dephased ensemble ($\zeta = 0.8$) in resonance with the cavity is shown. The cavity line width κ takes on values from 0.1 to 1.1 in units of κ_{crit}. Panel (a) shows the absolute value of the cavity amplitude, which is proportional to the number of photons inside the cavity. Panel (b) shows the evolution of the mean spin orientation along the z-axis. The purple line with $\kappa = 0.1\kappa_{crit}$ corresponds to the dynamical evolution in Figure 3.4 (a,b) starting from 2000 ns.

Jacobi matrix $\mathbf{J}(t)$:

$$\frac{d}{dt}\underbrace{\begin{pmatrix}\langle a\rangle\\ \langle\sigma_1^-\rangle\\ \vdots\\ \langle\sigma_N^-\rangle\end{pmatrix}}_{\mathbf{w}(t)} = \underbrace{\begin{pmatrix}-\kappa & -ig_1 & -ig_2 & \cdots & -ig_N\\ ig_1\zeta & -\alpha_1 & 0 & \cdots & 0\\ ig_2\zeta & 0 & -\alpha_2 & \cdots & 0\\ \vdots & \vdots & \vdots & \ddots & \vdots\\ ig_N\zeta & 0 & 0 & \cdots & -\alpha_N\end{pmatrix}}_{\mathbf{J}} \begin{pmatrix}\langle a\rangle\\ \langle\sigma_1^-\rangle\\ \vdots\\ \langle\sigma_N^-\rangle\end{pmatrix}. \tag{3.10}$$

Since $\mathbf{J}(t) \equiv \mathbf{J}$ is not time-dependent in this case, the solution of this differential equation is an exponential and we can analyze the stability of this system by examining the eigenvalues μ_i of $\mathbf{J}$. Global stability of the system is guaranteed, if the real part of all eigenvalues of $\mathbf{J}$ is negative [69], i.e.,

$$\mathrm{Re}(\mu_i) \leq 0, \quad \text{with } i = 0, \ldots, N. \tag{3.11}$$

Note, that in order to set up this matrix numerically we have to use the inhomogeneous coupling frequency discretization. Therefore, each line or column in $\mathbf{J}$ with entries g_k and α_k corresponds to a "large" spin with frequency Δ_k.

Next we compare this condition to the stability criterion found in Ref. [38]. To verify, that expressions 3.11 and 3.6 yield the same condition for stability, we calculate the eigenvalues of $\mathbf{J}$ for different values of κ numerically and compare

Die approbierte gedruckte Originalversion dieser Diplomarbeit ist an der TU Wien Bibliothek verfügbar
The approved original version of this thesis is available in print at TU Wien Bibliothek.

them to the values for the collective cooperativity, with the results being depicted in Figure 3.6. As can be seen in Figure 3.6, the collective cooperativity and the largest eigenvalue cross their respective critical value at exactly the same cavity line width κ.

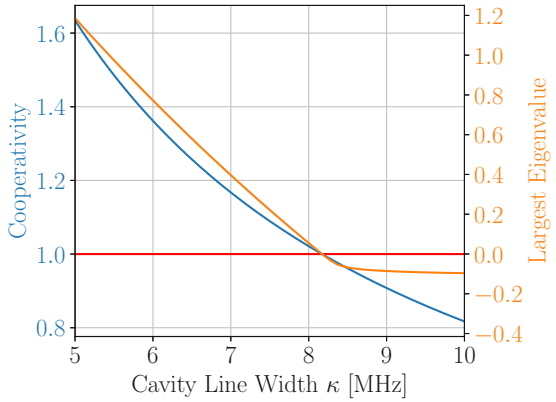

Figure 3.6. Comparison of the cooperativity (blue) to the numerically calculated largest eigenvalue of $\mathbf{J}$ (orange) for different values of κ.

Note that in the case of static stabilization, there is no real advantage in using condition (3.11) over the cooperativity criterion (3.6) derived in Ref. [38]. However, this calculation should serve as a basis for deriving stability conditions in periodically driven systems, where a similar approach using a Floquet ansatz is used.

3.3. External Pulse

The great challenge of stabilizing an inverted ensemble is to create a stable system, without decoupling it completely from the cavity. In general, a decoupling from the cavity wants to be avoided, since it abandons the ability to exchange information between the spin ensemble and its environment through the cavity. The interaction with the spin ensemble is usually done with an external electromagnetic pulse which is sent into the cavity. The external pulse transfers energy into the system, which leads to the excitation of spins in the cavity. Thereby the delicate balance in the stabilization mechanism can easily be obstructed, leading to the decay of the spin ensemble along with the release of the stored energy. In an ideal set up, the ensemble would release all its stored energy when it is hit by the external pulse.

For a physical understanding of this behavior, one can imagine the inverted spin ensemble as a pendulum that is carefully stabilized in its inverted position, using an arbitrary stabilization mechanism. While the pendulum should remain stable in the course of its free evolution, an external force should be able to overcome the

Die approbierte gedruckte Originalversion dieser Diplomarbeit ist an der TU Wien Bibliothek verfügbar
The approved original version of this thesis is available in print at TU Wien Bibliothek.

stabilization mechanism and tip it over, so it ends up in its ground state position after a few oscillations.

In the following, we probe the inverted spin ensemble with a small external driving pulse for cases when there is no stabilization mechanisms in place and in the case of a stabilized ensemble. We study the system's response to the external pulse and connect it to some real-world applications.

3.3.1. External Pulse without Stabilization

In a first analysis, we study a system with no stabilization mechanism, where the ensemble is strongly coupled to the cavity. We start again with an inversion of $\zeta = 0.8$ and employ the procedure to remove the global tipping angle, introduced in Section 3.1. By doing so, the ensemble stays inverted for a short period of time. The duration of this inverted position depends on the duration of the initial detuning and is strongly connected to the initial global tipping angle of the ensemble. In our simulation, the ensemble is detuned by 15 MHz for 2000 ns until the values for $\langle \sigma^x \rangle$ and $\langle \sigma^y \rangle$ approach their numerical precision limits close to 0, resulting in a completely dephased ensemble. After that, the spin ensemble is again tuned back to resonance with the cavity.

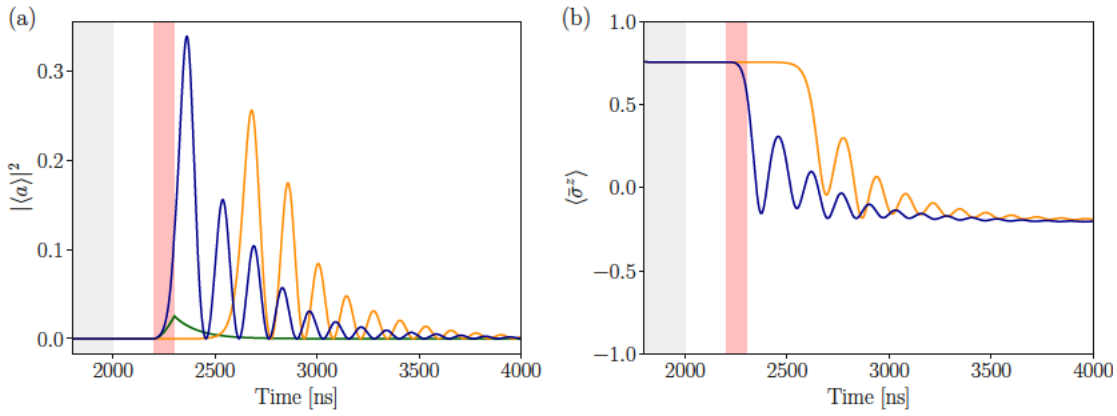

Figure 3.7. Response of a partially inverted spin ensemble to a weak probe pulse of 100 ns duration. The time in which the pulse is applied is marked by the red-shaded area between 2200 ns and 2250 ns. In the blue and orange lines, the ensemble is detuned for 2000 ns (gray shaded area), after which it is again tuned into resonance with the cavity. A pulse is then applied only to the ensemble represented by the blue line, showing a clear decay triggered by the external pulse, while the orange line shows an ensemble that decays by itself after $\sim$ 500 ns (no stabilization mechanism). For comparison, we show in (a) the effect of the same input pulse in an empty cavity (green line).

Die approbierte gedruckte Originalversion dieser Diplomarbeit ist an der TU Wien Bibliothek verfügbar
The approved original version of this thesis is available in print at TU Wien Bibliothek.

As can be observed in Figure 3.7, the ensemble undergoes a self-induced decay after ~ 500 ns. If, however, an external pulse is injected into the cavity during the period of inversion, a decay is triggered by the pulse and photons are emitted from the cavity superradiantly. This can be observed in Figure 3.7, where a 100 ns pulse is injected into the cavity, 200 ns after the ensemble is tuned back into resonance with the cavity. For comparison, we also show the effect of a pulse, injected into an empty cavity (green line in Figure 3.7 (a)). In this case, the pulse is not able to gain any energy in the cavity.

The decay of the spin ensemble is triggered after a critical cavity amplitude is reached. Thus, if the amplitude of the pulse is small enough, the pulse does not trigger the decay immediately as the critical level has not yet been reached. By measuring the delay between the decay and the applied pulse, one can deduce the amplitude of the pulse, which corresponds to the number of photons. This ability can be very useful in the context of a sensitive photo-detector. The relation between pulse strength and decay time delay can be seen in Figure 3.8.

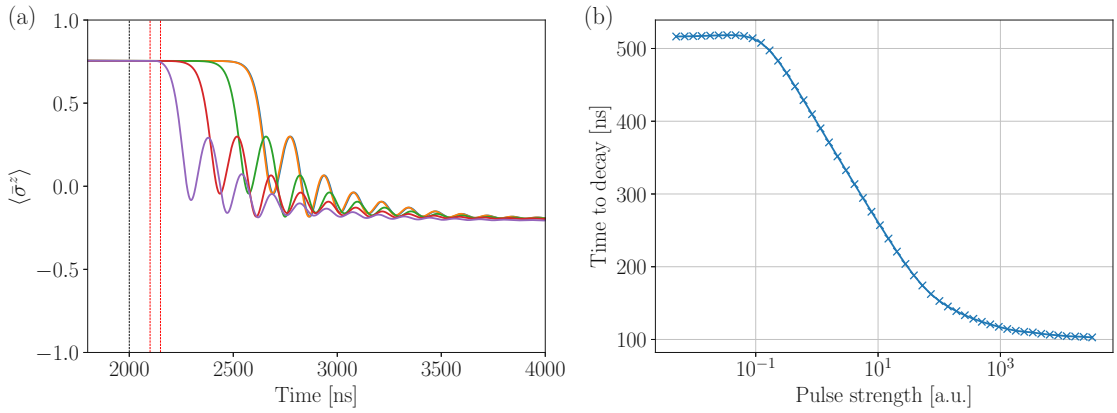

Figure 3.8. In panel (a), an external 50 ns pulse is shown as it is applied to the cavity for different pulse strengths. The ensemble is first detuned for 2000 ns and then brought back into resonance, where after the pulse is applied 100 ns later (in the period between the red dotted lines). The pulse strength takes on the values 0.1 (orange), 1 (green), 10 (red) and 100 (purple) in arbitrary units. The decay of the ensemble without an external pulse is also shown (blue), however it is mostly covered by the orange line. Panel (b) shows the relation between applied pulse strength and the time until the ensemble decays. The time of the decay is defined by the time $\langle\sigma^z\rangle$ varies by 1% of its initial value.

In this simulation, the cavity is set up similarly to the previous calculation. The ensemble is again detuned by 15 MHz for 2000 ns and then brought back into resonance (black vertical line in Figure 3.8). The 50 ns pulse is applied 100 ns after the ensemble is tuned back into resonance. By varying the pulse amplitudes,

Die approbierte gedruckte Originalversion dieser Diplomarbeit ist an der TU Wien Bibliothek verfügbar
The approved original version of this thesis is available in print at TU Wien Bibliothek.

we determine the time delay between the pulse and the decay for different drive strengths. We observe an exponential decrease of the time delay for increasing pulse strengths which is flattened towards the limiting time delay values.

The fact that a temporarily inverted ensemble can increase the energy of a small external pulse by a triggered decay shows great potential for an experimental realization of a photo detector which utilizes this inverted spin ensemble. With the relation between the time delay of the decay and the applied pulse strength, it is also possible to determine the number of incoming photons for a range of different pulse strengths.

3.3.2. External Pulse with Stabilization

Next, we consider a system, where the cavity line width κ is increased to the critical value κ_{crit}, such that we obtain a stable ensemble. Starting with a tipping angle corresponding to $\zeta = 0.8$, the ensemble is first detuned for a short period of time, in order to remove any global tipping angle, after which it is again tuned back into resonance with the cavity. Then, a series of weak probe pulses is injected into the cavity. To show that the observed pulse carries energy released by the spin ensemble, it is compared to the same sequence of pulses, applied to an empty cavity. The resulting system dynamics are depicted in Figure 3.9.

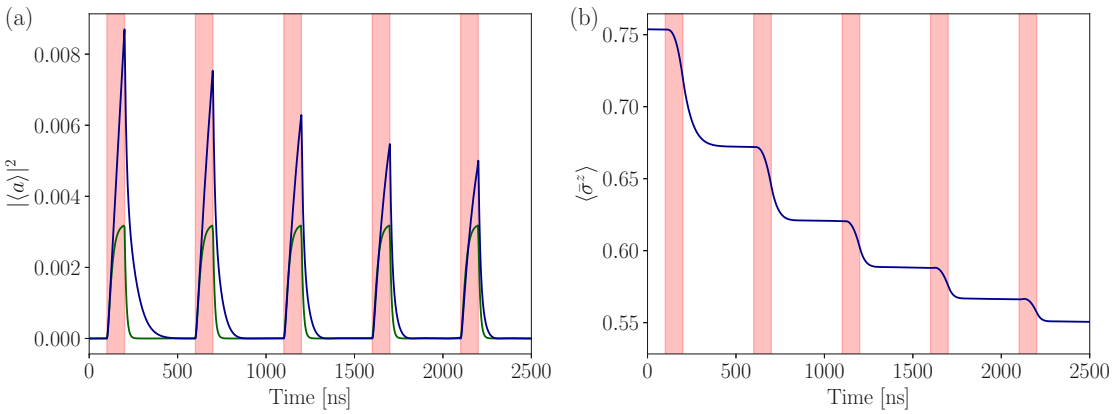

Figure 3.9. Response of a partially inverted spin ensemble to a series of weak probe pulses of 100 ns duration each. The time in which the pulse is applied is marked by the red-shaded areas. The blue line depicts the response of the stabilized ensemble with the cavity amplitude in (a) and the z-component of the average spin vector in (b). The green line shows the effect of the pulses in an empty cavity.

We observe by the increased cavity amplitude in the stabilized ensemble (blue line) compared to the empty cavity (green line), that the pulse is able to extract energy from the system. Since the ensemble only releases parts of its energy at

Die approbierte gedruckte Originalversion dieser Diplomarbeit ist an der TU Wien Bibliothek verfügbar
The approved original version of this thesis is available in print at TU Wien Bibliothek.
TU Bibliothek Your knowledge hub WIEN

each pulse, subsequent pulses are able to repeatedly extract energy. Such behavior is useful in the context of a quantum battery, where energy can be extracted repeatedly in a controlled manner.

Die approbierte gedruckte Originalversion dieser Diplomarbeit ist an der TU Wien Bibliothek verfügbar
The approved original version of this thesis is available in print at TU Wien Bibliothek.
TU Bibliothek Your knowledge hub WIEN

Chapter 4.

Dynamic Stabilization using Floquet Engineering

In this chapter we introduce a new method to stabilize an inverted spin ensemble inside a cavity. In this method, stabilization is achieved by periodically detuning the spins from the cavity. In other words, the spin ensemble is periodically coupled and decoupled from the cavity. As shown in the previous chapter, a detuned spin ensemble dephases over time, which leads to a stabilization mechanism. By periodically detuning the spins from the cavity we aim to obtain a stable ensemble, which can still be controlled via the cavity and thus allows for an exchange of information between the ensemble and the environment. The periodic detuning of the spins with amplitude A and frequency Θ are treated as follows:

$$\Delta_k = \omega_k - \omega_c \rightarrow \Delta_k'(t) = \omega_k + A\cos(\Theta t) - \omega_c. \tag{4.1}$$

In order to describe the dynamics of this system, we first give a short introduction to Floquet theory, a powerful framework for analyzing periodically driven systems. Following from this, we derive a condition for stability, given the amplitude and frequency of the periodic detuning. To get a better understanding of this mechanism and to explore the relevant physics of the stabilization effect, we apply this method to a system with only a single spin coupled to a cavity. Then we extend the stabilization procedure to a large ensemble of spins and finally show the effect of an external pulse on the stabilized inverted spin ensemble.

4.1. Floquet Theory

We start by giving a short introduction to classic Floquet theory [70]. Floquet theory was first introduced to describe the behavior of a set of linear differential equations with time-periodic coefficients

$$\dot{x} = \mathbf{A}(t)x, \quad t \in \mathrm{R},\ x \in \mathrm{R}^n, \tag{4.2}$$

where $\mathbf{A}(t)$ is a matrix, periodic in time with some period $T > 0$. The main theorem in Floquet theory relates every fundamental matrix $\mathbf{X}$ of the system to a canonical

Die approbierte gedruckte Originalversion dieser Diplomarbeit ist an der TU Wien Bibliothek verfügbar
The approved original version of this thesis is available in print at TU Wien Bibliothek.

representation

$$\mathbf{X}(t) = \mathbf{F}(t) \exp(t\mathbf{K}), \tag{4.3}$$

called the Floquet representation, where $\mathbf{F}(t)$ is some T-periodic matrix and $\mathbf{K}$ is some constant matrix. This gives a coordinate change $y = \mathbf{F}^{-1}(t)x$, that transforms the periodic system to a linear system with constant coefficients. Floquet theory is widely used in the stability analysis of dynamical systems. Most prominently, if applied to a potential which is periodic in space, Floquet theory provides the well known Bloch-States in solid state physics [71].

4.1.1. One-period Propagator

The one-period propagator $\mathbf{L}_0$, also defined as Floquet operator, is a crucial ingredient, when trying to analyze the stability of a linear periodic system. The eigenstates of this operator are called Floquet states and the corresponding eigenvalues form the quasi-energies of the system. To calculate the one-period propagator for our system, we first recall the system matrix $\mathbf{J}$ of the linearized Maxwell-Bloch equations in Eq. (3.10). In contrast to the static stabilization methods, we now assume time-periodic coefficients $\alpha(t) = \gamma_\perp + \Delta_k(t)$, where the spin transition frequency offset is modulated by

$$\Delta_k(t) = \omega_k + A\cos(\Theta t) - \omega_c. \tag{4.4}$$

The resulting matrix differential equation, also referred to as state equation, $\dot{\mathbf{w}}(t) = \mathbf{J}(t) \cdot \mathbf{w}(t)$ can be written as

$$\frac{d}{dt}\underbrace{\begin{pmatrix} a \\ \sigma_1^- \\ \vdots \\ \sigma_N^- \end{pmatrix}}_{\mathbf{w}(t)} = \underbrace{\begin{pmatrix} -\kappa & -ig_1 & -ig_2 & \cdots & -ig_N \\ ig_1\zeta & -\alpha_1(t) & 0 & \cdots & 0 \\ ig_2\zeta & 0 & -\alpha_2(t) & \cdots & 0 \\ \vdots & \vdots & \vdots & \ddots & \vdots \\ ig_N\zeta & 0 & 0 & \cdots & -\alpha_N(t) \end{pmatrix}}_{\mathbf{J}(t)} \begin{pmatrix} a \\ \sigma_1^- \\ \vdots \\ \sigma_N^- \end{pmatrix} \tag{4.5}$$

and thus gives rise to a periodic Jacobi matrix $\mathbf{J}(t) = \mathbf{J}(t+T)$ with period $T = 2\pi/\Theta$. The propagator $\mathbf{L}(t, t_0)$ connects the solutions of Eq. (4.5) at different times by

$$\mathbf{w}(t) = \mathbf{L}(t, t_0) \cdot \mathbf{w}(t_0). \tag{4.6}$$

Evidently, $\mathbf{L}(t, t_0)$ satisfies an entirely similar equation as Eq. (4.5), namely

$$\frac{d}{dt}\mathbf{L}(t, t_0) = \mathbf{J}(t) \cdot \mathbf{L}(t, t_0), \tag{4.7}$$

Die approbierte gedruckte Originalversion dieser Diplomarbeit ist an der TU Wien Bibliothek verfügbar
The approved original version of this thesis is available in print at TU Wien Bibliothek.
TU Bibliothek Your knowledge hub WIEN

whose formal solution is a time-ordered exponential series:

$$\mathbf{L}(t,t_0) = \mathrm{Texp}\left[\int_{t_0}^{t} dt' \mathbf{J}(t')\right] \overset{\text{def}}{=} \sum_{n=0}^{\infty} \frac{1}{n!} \int_{t_0}^{t} dt_1 \cdots \int_{t_0}^{t} dt_n \; \mathrm{T}\left[\mathbf{J}(t_1)\cdots\mathbf{J}(t_n)\right], \quad (4.8)$$

where $\mathrm{T}[\cdots]$ orders the "operators" with the prescription "later times to the left". Among the properties of the propagator, one can clearly see that $L(t_0,t_0)$ is the unit matrix. Also, it can be shown that propagators at different times can be connected by

$$\mathbf{L}(t_2,t_0) = \mathbf{L}(t_2,t_1)\cdot\mathbf{L}(t_1,t_0). \quad (4.9)$$

This becomes clear if one considers the solution of the state Eq. (4.6), fulfilling

$$\begin{aligned} \mathbf{w}(t_1) &= \mathbf{L}(t_1,t_0)\cdot\mathbf{w}(t_0), \\ \mathbf{w}(t_2) &= \mathbf{L}(t_2,t_1)\cdot\mathbf{w}(t_1) = \mathbf{L}(t_2,t_1)\cdot\mathbf{L}(t_1,t_0)\cdot\mathbf{w}(t_0). \end{aligned} \quad (4.10)$$

On the other hand

$$\mathbf{w}(t_2) = \mathbf{L}(t_2,t_0)\cdot\mathbf{w}(t_0) \quad (4.11)$$

and thus follows by uniqueness of the solution $\mathbf{w}(t)$:

$$\begin{aligned} \mathbf{L}(t_2,t_1)\cdot\mathbf{L}(t_1,t_0)\cdot\mathbf{w}(t_0) &= \mathbf{L}(t_2,t_0)\cdot\mathbf{w}(t_0) \\ \Longrightarrow\; \mathbf{L}(t_2,t_0) &= \mathbf{L}(t_2,t_1)\cdot\mathbf{L}(t_1,t_0). \end{aligned} \quad (4.12)$$

The Floquet operator $\mathbf{L}_0$ is defined as the one-period propagator which connects solutions over one period T of the system's Jacobi matrix

$$\mathbf{L}_0 \equiv \mathbf{L}(t_0,t_0+T). \quad (4.13)$$

Therefore, the dynamical evolution of the sampled solution $\mathbf{w}(k) = \mathbf{w}(t+kT)$ is governed by the time-invariant equation

$$\mathbf{w}(k) = (\mathbf{L}_0)^k \mathbf{w}(0). \quad (4.14)$$

This is why the eigenvalues of $\mathbf{L}_0$ play a major role in the stability analysis of periodic systems. By diagonalizing $\mathbf{L}_0$ one can find the $N+1$ eigenvectors, denoted by $\mathbf{u}_j(t_0)$, fulfilling

$$\mathbf{L}_0\cdot\mathbf{u}_j(t_0) = \mu_j\mathbf{u}_j(t_0) \quad \text{with } j=0,\ldots,N, \quad (4.15)$$

where $\mu_j \in \mathbb{C}$ in general. Note, that the eigenvalues are independent of t_0 and can thus be obtained for arbitrary t_0. Stability is guaranteed if the eigenvalues belong to the unit disk in the complex plane, fulfilling the condition

$$|\mu_j| \leq 1 \quad \forall j = 0,\ldots,N. \quad (4.16)$$

With this condition we are able to quantitatively classify periodically modulated system as stable or unstable. The time ordered-exponential series in the one-period propagator can in general only be calculated by numerical integration, making this again a condition that can only be decided numerically.

Die approbierte gedruckte Originalversion dieser Diplomarbeit ist an der TU Wien Bibliothek verfügbar
The approved original version of this thesis is available in print at TU Wien Bibliothek.
TU Bibliothek Your knowledge hub WIEN

4.2. Single Spin System

In order to get a better understanding for the stabilization mechanism we study a system with a single spin coupled to cavity. The resulting Maxwell-Bloch equations are reduced to a set of three non-linear differential equations with a single coupling strength g and transmission frequency offset $\Delta(t) = \omega + A\cos(\Theta t) - \omega_c$:

$$\langle \dot{a} \rangle = -\left(\kappa + i\Delta_c\right)\langle a \rangle - ig\langle \sigma^- \rangle, \tag{4.17}$$

$$\langle \dot{\sigma}^- \rangle = -\left(\gamma_h + 2\gamma_p + i\Delta(t)\right)\langle \sigma^- \rangle + ig\langle \sigma^z \rangle\langle a \rangle, \tag{4.18}$$

$$\langle \dot{\sigma}^z \rangle = -2\gamma_h\left(\langle \sigma^z \rangle + 1\right) - 4g\,\mathrm{Im}\left(\langle \sigma^- \rangle\langle a^\dagger \rangle\right). \tag{4.19}$$

4.2.1. Parameter Scan

With the previously introduced one-period propagator $\mathbf{L}_0$ we are able to analyze the stability of the system with regard to the modulation parameters A and Θ. After linearization of the corresponding Maxwell-Bloch equations, as described in Subsection 2.3.1, the Jacobi matrix of the single spin system is given by

$$\mathbf{J}(t) = \begin{pmatrix} -\kappa & -ig \\ ig & -(\gamma_\perp + i\Delta(t)) \end{pmatrix}, \tag{4.20}$$

with periodic modulation of the spin transition frequency as given by Eq. (4.4). Even for this simple 2×2 matrix, the one-period propagator can only be calculated numerically, due to the infinite time-ordered exponential series. However, since the system size is rather small, a quick numerical integration allows for a thorough parameter scan, where the detuning amplitude A and the detuning frequency Θ are varied and the resulting largest eigenvalue of the one-period propagator is recorded. The result of this calculation can be seen in Figure 4.1. The dark blue regions in Figure 4.1 depict the regions, where condition (4.16) is fulfilled and the system remains in its inverted position, while the yellow regions depict unstable modulation configurations.

To validate our results, we present in Figure 4.1 (b) the dynamical evolution of $\langle \sigma^z \rangle$ calculated by the Maxwell-Bloch Eqs. (4.17)-(4.19) for different points in a parameter scan. The points are chosen on a single detuning frequency, with one point residing in the stable region and the other ones with a higher and lower detuning amplitude as can be seen in Figure 4.2 (a). As expected, only for the configuration within the stable area, the spin stays inverted. Note that in contrast to the constant spin detuning, described in Subsection 3.1, here a larger detuning does not lead to a more stable system.

Die approbierte gedruckte Originalversion dieser Diplomarbeit ist an der TU Wien Bibliothek verfügbar
The approved original version of this thesis is available in print at TU Wien Bibliothek.
TU Bibliothek Your knowledge hub WIEN

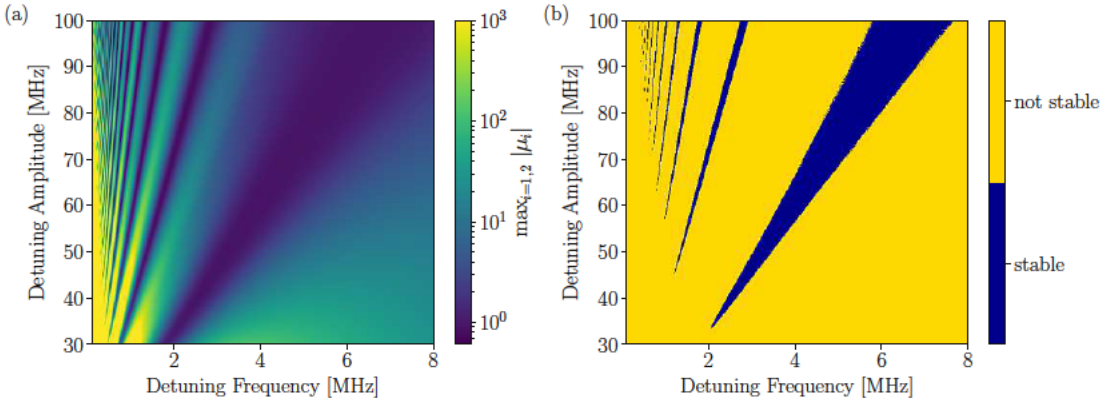

Figure 4.1. Panel (a) shows the result of the parameter scan for the absolute value of the largest eigenvalue in the one-period propagator of the single spin system. Panel (b) shows the points separated into stable and unstable regions, determined by condition (4.16).

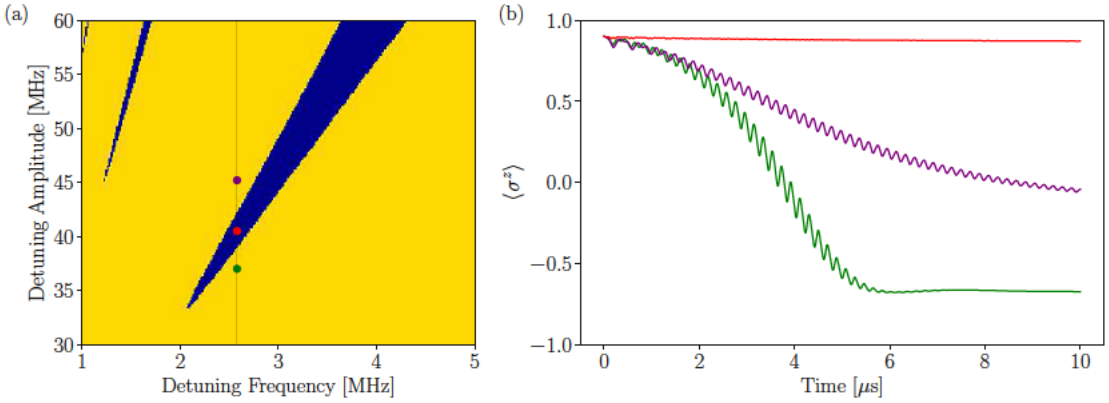

Figure 4.2. Panel (a) shows the chosen configurations of the modulated detuning used for the simulations in panel (b). The blue regions refer to stable configurations, while the system is unstable in the yellow region. The configuration points are chosen at a fixed modulation frequency $\Theta = 2.58$ MHz with different amplitudes $A = 37$ MHz (green), $A = 40.5$ MHz (red) and $A = 45.2$ MHz (purple). The colors of the configurations correspond to the colors in the simulated evolution of $\langle \sigma^z \rangle$, shown in panel (b).

Die approbierte gedruckte Originalversion dieser Diplomarbeit ist an der TU Wien Bibliothek verfügbar
The approved original version of this thesis is available in print at TU Wien Bibliothek.

4.2.2. Stabilization Mechanism

To get a better understanding of this stabilization mechanism we analyze the single spin system in more detail using Equations (4.17)-(4.19). Here, for simplicity, we neglect any system losses through individual spin dissipations ($\gamma_h = \gamma_p = 0$). This leaves us with the following simplified set of equations

$$\langle \dot{a} \rangle = -\kappa \langle a \rangle - ig \langle \sigma^- \rangle, \tag{4.21}$$

$$\langle \dot{\sigma}^- \rangle = -i\Delta \langle \sigma^- \rangle + ig \langle \sigma^z \rangle \langle a \rangle, \tag{4.22}$$

$$\langle \dot{\sigma}^z \rangle = -4g \,\mathrm{Im}\left(\langle \sigma^- \rangle \langle a^\dagger \rangle \right). \tag{4.23}$$

To show the effect of a constant detuning, we consider an isolated spin without cavity, with a transition frequency offset $\Delta > 0$

$$\langle \dot{\sigma}^- \rangle = -i\Delta \langle \sigma^- \rangle. \tag{4.24}$$

Using the Pauli operator relation (2.2) we solve Eq. (4.24) to

$$\langle \sigma_x \rangle + i \langle \sigma_y \rangle \propto e^{-i\Delta t} = \cos(\Delta t) - i \sin(\Delta t). \tag{4.25}$$

From this one can see, that a detuning from the central cavity frequency, rotates the spin around the z-axis with rotation frequency $\Delta/2\pi$. A periodically modulated detuning thus corresponds to periodically increasing and decreasing this rotation frequency.

Next, we assume a stable system, where $\langle \dot{\sigma}^z \rangle = 0$ is naturally satisfied. Together with Eq. (4.23) this can be rearranged to the following expression

$$-4g \,\mathrm{Im}\left(\langle \sigma^- \rangle \langle a^\dagger \rangle \right) = 0 \quad \Longleftrightarrow \quad a_{\mathrm{Re}} \sigma_y + a_{\mathrm{Im}} \sigma_x = 0, \tag{4.26}$$

where $a_{\mathrm{Re}} = \mathrm{Re}(a)$ and $a_{\mathrm{Im}} = \mathrm{Im}(a)$. This condition is fulfilled exactly when the phase difference between the spin and the field inside the cavity is 0 or π.

Note that the phase relation in Eq. (4.26) is closely related the concept of superradiance and superabsorption [35, 72–74]. Superradiance refers to a process of cooperative emission of light in a dense collection of atoms. Interatomic correlations allow atoms to align their individual dipoles to form one giant dipole moment, which lets them emit photons faster than individual atoms. Such correlations do not have to be externally imposed, but can also be self-induced by the decay process of an excited state, as is the case for the spin ensemble coupled to a cavity. Importantly, the phase of the field emitted into the cavity during the superradiant emission is linked to the phase of the collective spin state during this process. The time reversed process of superradiance also exists and is known as superabsorption [35, 72–74]. Superabsorption implies that the rate of absorbed photons is enhanced compared to a collection of individual atoms. Theoretically, the difference between superabsorption and superradiance in the spin ensemble is simply a

Die approbierte gedruckte Originalversion dieser Diplomarbeit ist an der TU Wien Bibliothek verfügbar
The approved original version of this thesis is available in print at TU Wien Bibliothek.
TU Bibliothek Your knowledge hub WIEN

π phase shift in the cavity field or the spins. In other words, if the phase between the spins and the field is chosen opposite to the phase of a superradiantly emitted pulse, the cavity field is (super)absorbed by the ensemble.

If we translate this to our single spin system, we can observe a similar effect by instantaneously switching the phase between the spin and the cavity during the decay of the spin. To demonstrate this, we prepare an inverted spin state inside the cavity with a small tipping angle along the y-axis. Due to this small tipping angle the spin starts to decay and rotates downwards on the Bloch sphere along the y-z-plane creating a field in the cavity. The phase of this field is given by the phase of the spin in the x-y-plane with an additional $-\pi/2$ offset. As an example we consider again an inverted spin which is slightly tipped by a small rotation along the y-axis. If after some time of free evolution, we externally switch the cavity field phase from $-\pi/2$ to $\pi/2$, the spin no longer rotates downwards but rotates upwards again, absorbing the field just emitted, as presented in Figure 4.3. The spin continues to rotate upwards until all of the remaining field inside the cavity is absorbed, after which the emission starts again. Thereafter, the spin oscillates due to the well-known Rabi oscillations, occurring from the strong coupling of the spin to the cavity.

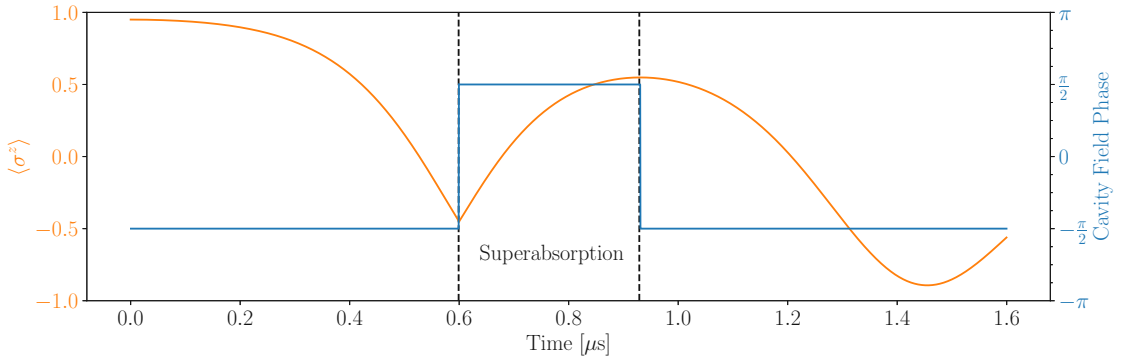

Figure 4.3. The effect of an instantaneous switch in the phase of the cavity field is shown. The spin is initially prepared as inverted spin, tipped in the x-direction. Thus, it rotates during its decay solely in the x-z-plane, i.e. with phase 0. Therefore the emerging cavity field obtains the phase $-\pi/2$. At 0.6 μs the phase is instantaneously switched by π, resulting in the spin suddenly rotating in its opposite direction until it has absorbed all energy from the cavity, after which it decays again.

In a stable system, we want neither emission nor absorption to occur. This is captured in Eq. (4.26), where the phase between spin and field is either 0 or π, which is exactly in between emission and absorption. To demonstrate this behavior, we study the dynamics presented in Figure 4.2 in more detail. In particular, we show the relative phase between the cavity field and the spin, denoted by $\Delta\varphi$. Naturally,

Die approbierte gedruckte Originalversion dieser Diplomarbeit ist an der TU Wien Bibliothek verfügbar
The approved original version of this thesis is available in print at TU Wien Bibliothek.
TU Bibliothek Your knowledge hub WIEN

$\Delta\varphi$ can have values $-\pi \leq \Delta\varphi \leq \pi$ and similar to the above consideration, the spin emits energy into the cavity if $\Delta\varphi < 0$ and absorbs energy from the cavity if $\Delta\varphi > 0$. In order to better visualize this behavior, we show $\sin(\Delta\varphi)$, which reaches the value 0 for $\Delta\varphi = 0$ and $|\Delta\varphi| = \pi$, while leaving the previous considerations unchanged. Additionally, we show the value of $a_{\mathrm{Re}}\sigma_y + a_{\mathrm{Im}}\sigma_x$ over time, which is proportional to the change in $\langle\sigma^z\rangle$ and thus is expected to stay close to 0 in a stable system. In Figure 4.4 we compare the values of $\sin(\Delta\varphi)$ and $a_{\mathrm{Re}}\sigma_y + a_{\mathrm{Im}}\sigma_x$ for the three different configurations chosen in Figure 4.2. We observe a qualitative difference

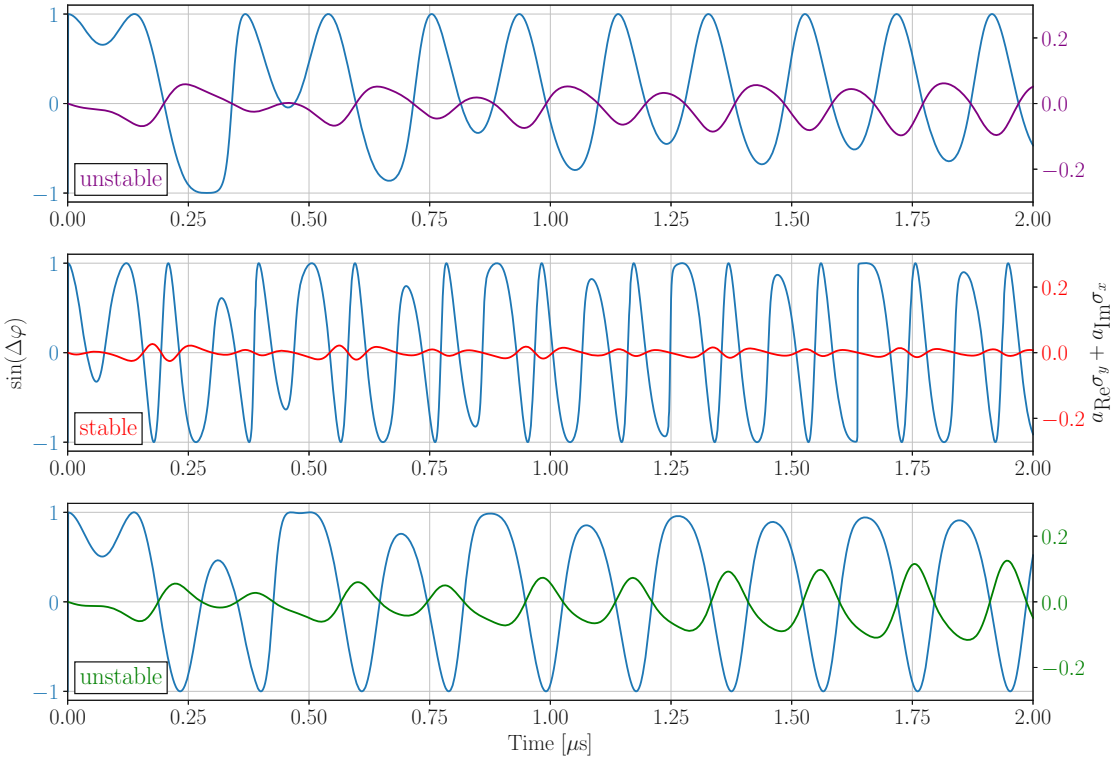

Figure 4.4. The relative phase between cavity field and spin $\Delta\varphi$ is shown as $\sin(\Delta\varphi)$ by the blue line together with the values for $a_{\mathrm{Re}}\sigma_y + a_{\mathrm{Im}}\sigma_x$. The colors correspond to the configurations in Figure 4.2, where red resembles a stable configuration and green and purple are unstable configurations.

between the stable and unstable configurations already in the first few hundred nanoseconds. While in the unstable systems (purple and green in Figure 4.4), the spin emits energy over the whole first 200 nanoseconds, the stable system already switches between emission and absorption a few times. The fast switching between emission and absorption within the stable region forces the value of $a_{\mathrm{Re}}\sigma_y + a_{\mathrm{Im}}\sigma_x$ more often to 0 and hence allows only smaller changes in $\langle\sigma^z\rangle$.

Over the course of the whole decay, $a_{\mathrm{Re}}\sigma_y + a_{\mathrm{Im}}\sigma_x$ reaches larger values in the

Die approbierte gedruckte Originalversion dieser Diplomarbeit ist an der TU Wien Bibliothek verfügbar
The approved original version of this thesis is available in print at TU Wien Bibliothek.

unstable systems and, since it is proportional to the change in $\langle \sigma^z \rangle$, leads to a larger deviation of $\langle \sigma^z \rangle$ from its initial inverted value. This can be observed in Figure 4.5, where we compare the values of $a_{\mathrm{Re}}\sigma_y + a_{\mathrm{Im}}\sigma_x$ in the unstable and stable configurations over time. In the latter case, the value of $a_{\mathrm{Re}}\sigma_y + a_{\mathrm{Im}}\sigma_x$ remains significantly smaller than for the unstable systems.

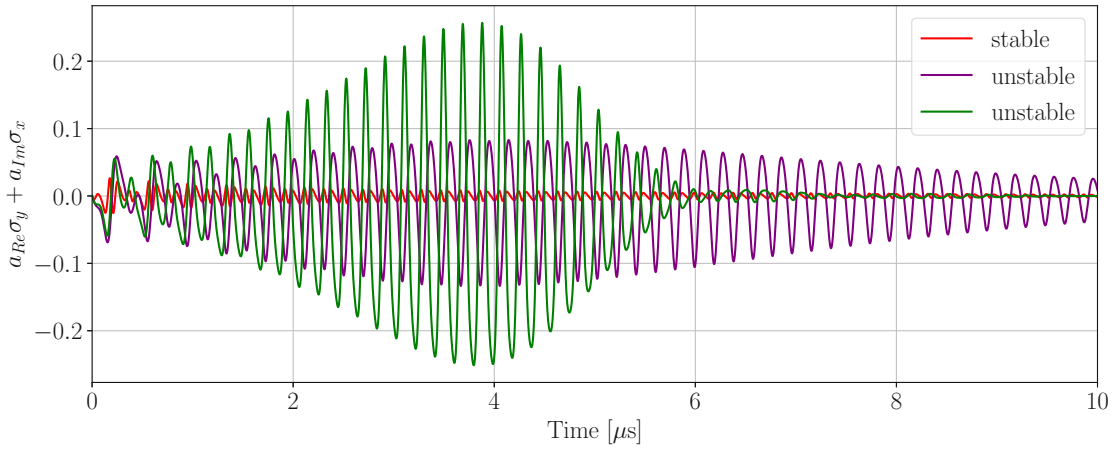

Figure 4.5. The term $a_{\mathrm{Re}}\sigma_y + a_{\mathrm{Im}}\sigma_x$, derived in Eq. (4.26), is shown for the three configurations presented in Figure 4.2 with the corresponding colors.

4.3. Spin Ensemble

While the small system size in the single spin system allows for a quick calculation of the one-period propagator and thus a very precise parameter scan, we have to choose a coarser grid for the ensemble with N spins. The one-period propagator $\mathbf{L}_0$ is calculated by numeric integration of Eq. (4.7), with the periodic Jacobi matrix $\mathbf{J}(t) = \mathbf{J}(t+T)$ and the initial condition $t_0 = 0$ chosen for convenience. This way, we again calculate $\mathbf{L}_0$ for various values of the modulation amplitude A and the modulation frequency Θ and record the maximal eigenvalue depicted in Figure 4.6. Here, we observe some similarities with the spectrum of the single spin system shown in Figure 4.1. However, the region of stability now spans over almost all lower detuning frequencies with a minimal detuning amplitude of around 25 MHz. For detuning frequencies $\Theta > 5$ MHz a narrow band of instability can be observed, where the absolute value the largest eigenvalue in this region exceeds one.

In Figure 4.7, we compare the dynamic evolution of the inverted spin ensemble in the stable as well as in the unstable configuration space by numerically solving the full Maxwell-Bloch equations.

First, a case with detuning frequency $\Theta = 2$ MHz is shown, with two different amplitudes $A = 17$ MHz and 30 MHz. In agreement with our stability analysis

Die approbierte gedruckte Originalversion dieser Diplomarbeit ist an der TU Wien Bibliothek verfügbar
The approved original version of this thesis is available in print at TU Wien Bibliothek.

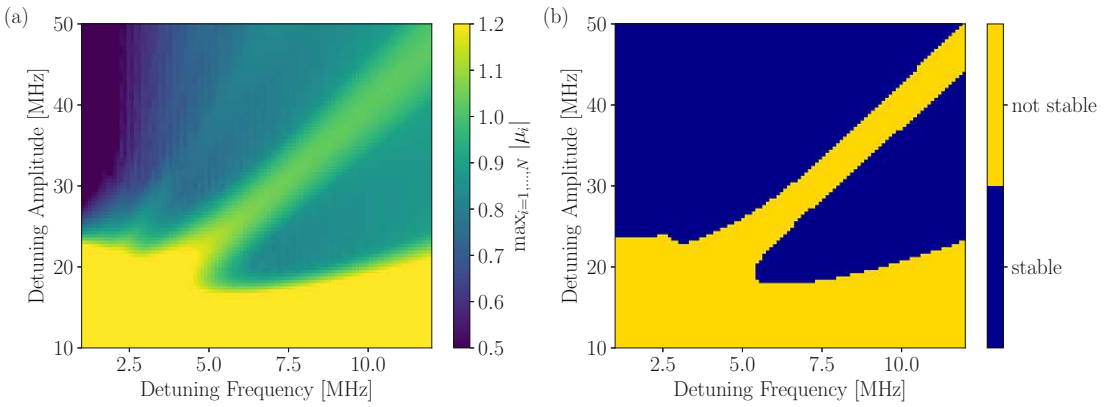

Figure 4.6. Parameter scan for the spin ensemble. In panel (a) the spectrum of the largest eigenvalue in $\mathbf{L}_0$ for various values of A and Θ is shown. Panel (b) shows the parameter space split into stable and unstable regions, determined by condition (4.16).

presented in Figure 4.6, we observe a significant emission of photons accompanied by a drastic decrease in the average spin expectation value for $A = 17$ MHz (unstable region), while for $A = 30$ MHz (stable region) no photon pulse is emitted and the the ensemble remains inverted.

Similarly, we choose a detuning frequency $\Theta = 6.5$ MHz and select two different amplitudes, $A = 27.7$ MHz (stable region) and $A = 21$ MHz (unstable region). Note however, that the eigenvalue in the narrow band of instability at $A = 27.74$ MHz exceeds one only marginally. Thus, the observed decay releases only a small margin of the energy stored in the ensemble. Nevertheless, we observe again a qualitative difference in the dynamics of the system for the two regions in perfect accordance with our stability analysis. The observed small decrease in $\langle \bar{\sigma}^z \rangle$ in the stable system (red line in Figure 4.7(d)) can be attributed to a relatively small individual spin decay according to the T_1 relaxation.

Die approbierte gedruckte Originalversion dieser Diplomarbeit ist an der TU Wien Bibliothek verfügbar
The approved original version of this thesis is available in print at TU Wien Bibliothek.

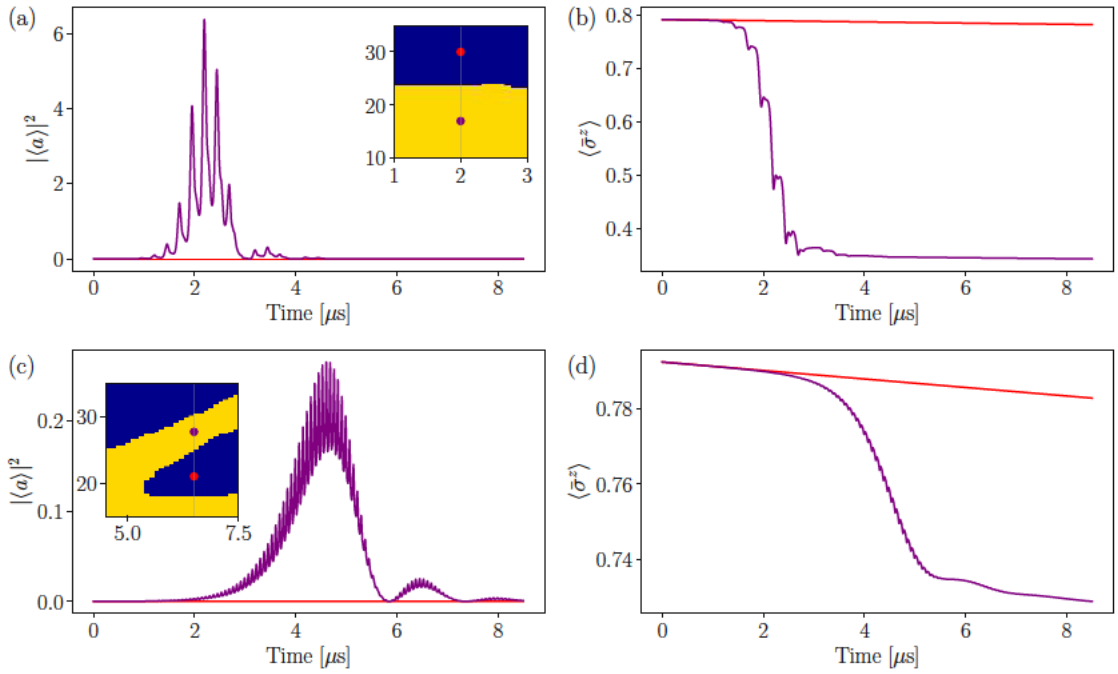

Figure 4.7. The dynamics of the cavity probability amplitude $|\langle a \rangle|^2$ (a,c) and the average spin expectation value $\langle \bar{\sigma}^z \rangle$ (b,d) for different points in the configuration space, are shown. In (a) and (b), the red line depicts a system with a periodic detuning frequency of $\Theta = 2$ MHz and an amplitude of $A = 30$ MHz. According to the parameter scan of the one-period propagator, such a detuning leads to a stable system, as can be seen by the red dot residing in the blue area in the inset of panel (a). By decreasing the amplitude to $A = 17$ MHz while keeping the same detuning frequency, the system enters the unstable region of the configuration space, as can be observed by the purple dot. Similarly, the dynamics of two systems with a modulation of $\Theta = 6.5$ MHz and $A = 21$ MHz (red), $A = 27.7$ MHz (purple), residing near the narrow band region is shown in (c) and (d). The decay here is, however, relatively small, as the unstable narrow band (see Figure 4.6) is characterized by eigenvalues only slightly exceeding unity.

4.3.1. External Pulse

Similarly to the external pulse for the statically stabilized ensemble, as described in Section 3.3, we want to analyze the behavior of the periodically detuned ensemble under the influence of an external pulse. For this reason, we prepare an inverted ensemble with $\zeta = 0.8$ and detune it for a short period of time resulting in a slightly dephased ensemble. Then a periodic modulation of the detuning frequency is applied which stabilizes the system in its inverted position, as discussed in the previous section.

Die approbierte gedruckte Originalversion dieser Diplomarbeit ist an der TU Wien Bibliothek verfügbar
The approved original version of this thesis is available in print at TU Wien Bibliothek.

We start with a system, which is periodically modulated only slowly, compared with the system's intrinsic time scales. We apply a periodic modulation with a frequency of $\Theta = 1$ MHz and an amplitude of $A = 25$ MHz. We then apply a short external pulse with a duration of 100 ns. Since the duration of the external pulse is much shorter than the period of the modulation, we observe different behaviors in the system, depending on the point of time, when the pulse is applied. In general, we can differentiate between two extremal cases: (i) First, the pulse is applied at a time, when the modulation crosses zero and thus the ensemble is in resonance with the cavity. (ii) Second, the pulse is applied when the modulation reaches one of its extremal points, where the system is the most detuned from the cavity. These two cases can be observed in Figure 4.8 (a), where one pulse is applied at 0.75 μs and one at 1 μs. The emerging system dynamics can be seen in Figure 4.8 (b) and (c).

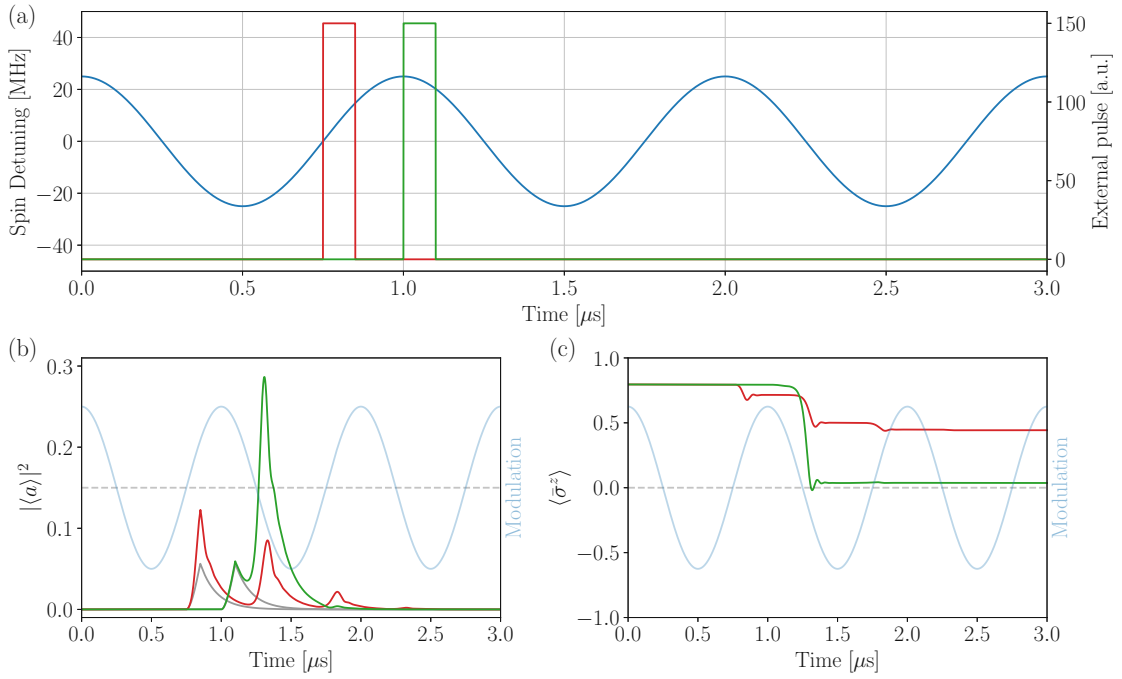

Figure 4.8. Demonstration of an external pulse in a "slowly" modulated system. The modulation of the system can be seen in panel (a) with a modulation frequency of $\Theta = 1$ MHz and an amplitude of $A = 25$ MHz. Two systems with different pulses are shown in panels (b) and (c). The system to which a pulse is applied when the ensemble is in resonance with the cavity is shown by the red line, while the system with the off-resonant pulse is shown by the green line. For comparison, the same pulses in an empty cavity are depicted by gray lines. The starting time of the pulses relative to the system modulation can also be seen in panel (a).

Die approbierte gedruckte Originalversion dieser Diplomarbeit ist an der TU Wien Bibliothek verfügbar
The approved original version of this thesis is available in print at TU Wien Bibliothek.

In the first case, where the pulse is applied when the ensemble is in resonance with the cavity, we observe an oscillating behavior in the cavity amplitude. When the pulse is applied, the ensemble quickly reaches its critical point and starts to decay. However, the periodic modulation then detunes the ensemble again, allowing for no possible decay channels. Only when the ensemble is tuned back into resonance we again observe a small decay with the excess energy. The dynamics repeats until the system again stabilizes after some time. Note that there is still some inversion left in the spin ensemble such that an additional external pulse would again be able to extract energy from the system.

For the second case, where the pulse is applied when the ensemble is most detuned from the cavity, we observe a different behavior. When the pulse is first applied, the ensemble is detuned from the cavity and thus the emerging dynamics correspond to that of a pulse in an almost empty cavity. To illustrate this, the pulse in an empty cavity is also depicted in Figure 4.8 (b) with a gray line. However, when the ensemble is tuned back into resonance, the field of the pulse which is still present in the cavity leads to a decay of the ensemble. The decay proceeds until the periodic modulation of the system again detunes the ensemble from the cavity. Since the allowed decay time after the pulse is first applied, is longer than in the first case, the pulse is able to harvest more energy from the ensemble.

To compare energy output of both cases we analyze the number of radiating photons. This is proportional to the integral of the cavity amplitude. In the example shown above, the number of emitted photons by the off-resonant pulse is increased by a factor of roughly 1.67 compared to the pulse on resonance. We note here, that this example for an external pulse in a "slowly" modulated system should simply serve as demonstration of different behaviors depending on the timing of a pulse relative to the system modulation. The exact dynamics of the system strongly depends on many parameters of both the external pulse (duration, strength) and the system itself.

Next, we analyze the dynamics of an external pulse in a system with "fast" modulation, where the modulation period is in the same range as the pulse duration. For this reason, we again start with an inverted and initially detuned ensemble and apply a periodic modulation with frequency $\Theta = 6.5$ MHz and amplitude $A = 21$ MHz, thus residing in the stable region of the parameter scan, as was shown in Figure 4.7. Then we apply a pulse with duration 100 ns to two systems at different points in time. The timing of the pulse relative to the modulation and the resulting dynamics can be seen Figure 4.9. We observe now generally fewer photons in the cavity, resulting from the external pulse. This is expected since the system now experiences more detuning during the pulse and thus there is less interaction between cavity and spin ensemble. Therefore, the resulting cavity amplitude of the pulse, compared to a pulse in an empty cavity (gray line in Figure 4.9 (b)) is only slightly increased. However, since the pulse duration is now in the order of the modulation period, we observe a smaller difference in the behavior depending on

Die approbierte gedruckte Originalversion dieser Diplomarbeit ist an der TU Wien Bibliothek verfügbar
The approved original version of this thesis is available in print at TU Wien Bibliothek.
TU Bibliothek Your knowledge hub WIEN

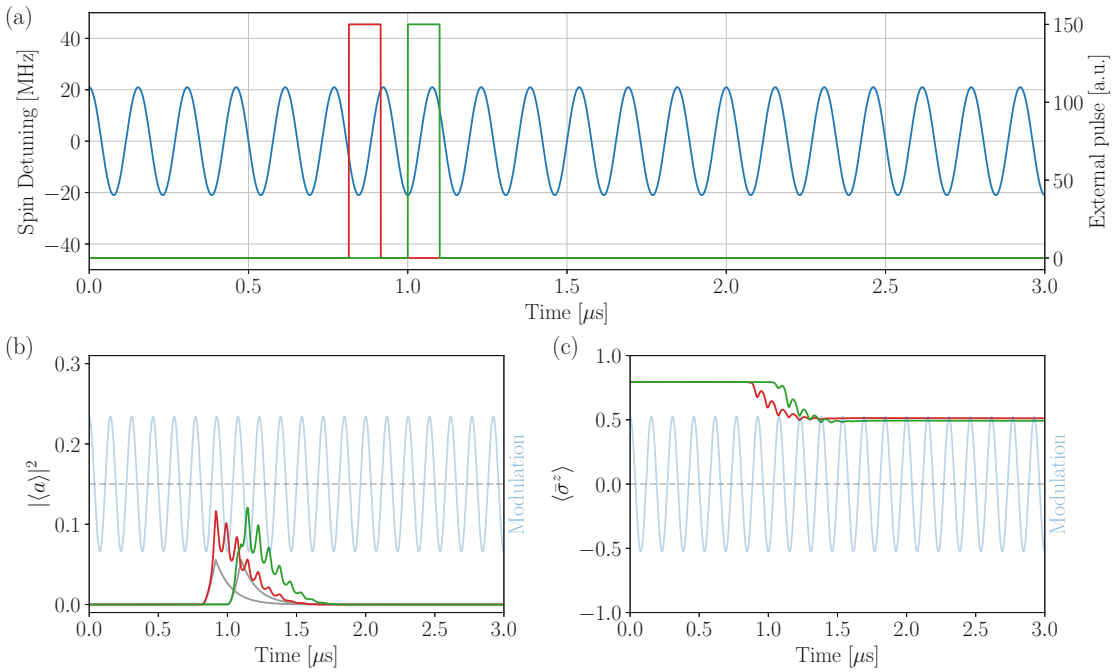

Figure 4.9. Demonstration of an external pulse in a "fast" modulated system. The modulation of the system can be seen in panel (a) with a modulation frequency of $\Theta = 6.5$ MHz and an amplitude of $A = 21$ MHz. Two systems with different pulses are shown in panels (b) and (c). The system where the pulse is applied when the ensemble is in resonance with the cavity is shown by the red line, while the system with the off-resonant pulse is shown by the green line. For comparison, the same pulses in an empty cavity are depicted by gray lines. The starting time of the pulses relative to the system modulation can also be seen in panel (a).

the timing of the pulse. The fact that the ensemble does not release all its energy when hit by a single pulse suggests that an additional pulse could again extract energy from the system. This can be observed in Figure 4.10, where a series of pulses, equal to the above, is injected into the cavity. By comparison of the cavity amplitudes of the inverted ensemble and the pulse in an empty cavity (gray line in Figure 4.10), we observe a significant increase in the first pulse and also a slight increase in the subsequent pulses.

Die approbierte gedruckte Originalversion dieser Diplomarbeit ist an der TU Wien Bibliothek verfügbar
The approved original version of this thesis is available in print at TU Wien Bibliothek.

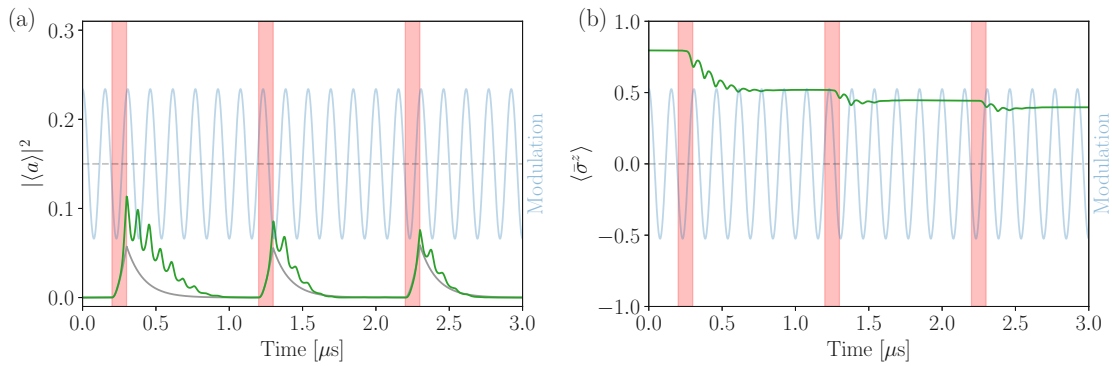

Figure 4.10. Response of a partially inverted spin ensemble with dynamic stabilization to a series of weak probe pulses of 100 ns duration each. The time in which the pulse is applied is marked by the red-shaded areas. The green line depicts the response of the stabilized ensemble with the cavity amplitude in (a) and the z-component of the average spin vector in (b). For comparison, the gray line shows the effect of the pulses in an empty cavity.

Die approbierte gedruckte Originalversion dieser Diplomarbeit ist an der TU Wien Bibliothek verfügbar
The approved original version of this thesis is available in print at TU Wien Bibliothek.

Chapter 5.

Summary and Outlook

In this thesis, we studied the stabilization of an inverted hybrid quantum system, consisting of an ensemble of spins coupled to a cavity. We have presented a way of stabilizing the inverted ensemble in two different ways. First, we demonstrated a method of static stabilization and then we introduced a periodic modulation of the system in a Floquet-based manner. Moreover, we showed how to distinguish between stable and unstable configurations.

Starting from a quantum mechanical description given by the Tavis-Cummings Hamiltonian, we derived the semiclassical Maxwell-Bloch equations, which form the basis of simulations in this thesis. By using an approximation similar to the Holstein-Primakoff transformation, we linearized the Maxwell-Bloch equations, allowing us to analyze the stability of the given system. We introduced the concept of a global tipping angle and demonstrated that by removing it, the decay of the system can be delayed for a short amount of time. Following from that, we showed a method of static stabilization, by decreasing the system cooperativity parameter, as suggested by Julsgaard and Mølmer [38].

Furthermore, we introduced a periodic modulation in the spin transition frequencies, which acts as a stabilization mechanism for the inverted ensemble. With the help of Floquet theory, we calculated the one-period propagator, which allows us to distinguish between stable and unstable configurations, depending on the modulation parameters such as amplitude and frequency. The resulting phase diagram was calculated for a single spin system, where it can be easily validated with the corresponding system dynamics. Additionally, the single spin system allows us to study the underlying stabilization mechanism, revealing a delicate balance between emission and absorption. This is expressed by the fact that the phase between the cavity field and the spin vector has to be either 0 or π. Only in these cases, the system neither absorbs, nor emits photons and thus the ensemble is able to remain in its inverted position. We then applied this stability analysis to the large spin ensemble and obtained a similar diagram of stable and unstable region in the configuration space.

Additionally, we simulated the effect of an external probing pulse on a stabilized system. We observed that in the stabilized ensemble, the pulse was able to extract

Die approbierte gedruckte Originalversion dieser Diplomarbeit ist an der TU Wien Bibliothek verfügbar
The approved original version of this thesis is available in print at TU Wien Bibliothek.
TU Bibliothek Your knowledge hub WIEN

energy from the inverted spin ensemble.

At the time of writing this thesis, the realization of an inverted spin ensemble and its stabilization is being implemented in the group of Jörg Schmiedmayer at the Atominstitut of TU Wien using NV centers in diamond coupled to a superconducting microwave resonator. With this experimental setup, one could verify the stability analysis carried out in this thesis. Achieving a stable inverted spin ensemble, which is capable to interact through the cavity by an external pulse could provide a basis for a range of practical applications like quantum batteries or weak microwave signal detectors.

Future studies in the theoretical analysis of the periodic modulation might focus on the effect of other system parameters on the stability of the inverted ensemble. Using these additional parameters, it would be desirable to accomplish to stabilize the spin ensemble already at a lower detuning frequency and amplitude, such that a strong response to an external pulse can be realized. For the optimally controlled release of stored energy in an inverted ensemble, stabilized by periodic modulation, one could also explore the effect of complex external pulses, rather than simple rectangular pulses as studied here.

Die approbierte gedruckte Originalversion dieser Diplomarbeit ist an der TU Wien Bibliothek verfügbar
The approved original version of this thesis is available in print at TU Wien Bibliothek.
TU Bibliothek Your knowledge hub WIEN

Appendix A.

Deriving the Maxwell-Bloch Equations

We give here a more detailed description of deriving the Maxwell-Bloch equations (2.8)-(2.10). First, we transform the Tavis-Cummings Hamiltonian (2.4) into the rotating frame ω_p to remove the explicit time-dependence in the external driving term. This transformation represents a unitary transformation by the means of

$$\tilde{H} = UHU^\dagger + i\frac{\partial U}{\partial t}U^\dagger, \tag{A.1}$$

where

$$U = e^{i\omega_p\left(a^\dagger a + \sum_k \frac{1}{2}\sigma_k^z\right)} = e^{i\omega_p a^\dagger a} e^{i\omega_p \sum_k \frac{1}{2}\sigma_k^z} = U_a U_\sigma, \tag{A.2}$$

yielding

$$\begin{aligned}\tilde{H} &= UHU^\dagger + i\left(i\omega_p(a^\dagger a + \sum_{k=1}^{N}\frac{1}{2}\sigma_k^z)\right)UU^\dagger \\ &= UHU^\dagger - \omega_p a^\dagger a - \sum_{k=1}^{N}\frac{1}{2}\sigma_k^z.\end{aligned} \tag{A.3}$$

In order to evaluate the term $UHU^\dagger$, we first use the series expansion of the exponential function $e^x = 1 + x + \frac{x^2}{2} + \ldots$ and the fact that $[a^\dagger a, a^\dagger a] = 0$ to find $[a^\dagger a, U_a] = 0$. Additionally, we note that a and σ_k^z act on different Hilbert spaces and thus trivially commute, from which follows $[a^\dagger a, U_\sigma] = 0$ and thus $[a^\dagger a, U] = 0$. This simplifies the evaluation of the first two term in $UHU^\dagger$, so we end up with

$$\begin{aligned}UHU^\dagger = {} & \omega_c a^\dagger a + \frac{1}{2}\sum_{k=1}^{N}\omega_k\sigma_k^z \\ & + i\sum_{k=1}^{N} g_k\left(U_\sigma\sigma_k^- U_\sigma^\dagger U_a a^\dagger U_a^\dagger + U_\sigma\sigma_k^+ U_\sigma^\dagger U_a a U_a^\dagger\right) \\ & + i\left[\eta(t)U_a a^\dagger U_a^\dagger e^{-i\omega_p t} - \eta(t)^* U_a a U_a^\dagger e^{i\omega_p t}\right].\end{aligned} \tag{A.4}$$

Die approbierte gedruckte Originalversion dieser Diplomarbeit ist an der TU Wien Bibliothek verfügbar
The approved original version of this thesis is available in print at TU Wien Bibliothek.
TU Bibliothek Your knowledge hub WIEN

Next, we evaluate the terms $U_\sigma \sigma_k^- U_\sigma^\dagger$, $U_\sigma \sigma_k^+ U_\sigma^\dagger$, $U_a a U_a^\dagger$ and $U_a a^\dagger U_a^\dagger$ individually, by utilizing the combinatorial lemma [75]

$$e^A B e^{-A} = B + [A,B] + \frac{1}{2!}[A,[A,B]] + \frac{1}{3!}[A,[A,[A,B]]] + \dots . \tag{A.5}$$

Together with commutation relations (2.1) and (2.2) we get

$$\begin{aligned} U_\sigma \sigma_k^- U_\sigma^\dagger &= e^{i\omega_p t \frac{1}{2}\sigma_k^z} \sigma_k^- e^{-i\omega_p t \frac{1}{2}\sigma_k^z} \\ &= \sigma_k^- + \frac{i\omega_p t}{2}\left[\sigma_k^z, \sigma_k^-\right] + \frac{1}{2!}\left(\frac{i\omega_p t}{2}\right)^2 \left[\sigma_k^z, \left[\sigma_k^z, \sigma_k^-\right]\right] + \dots \\ &= \sigma_k^- \sum_{n=0}^{\infty} \frac{1}{n!}(-i\omega_p t)^n = \sigma_k^- e^{-i\omega_p t}, \end{aligned} \tag{A.6}$$

$$\begin{aligned} U_\sigma \sigma_k^+ U_\sigma^\dagger &= e^{i\omega_p t \frac{1}{2}\sigma_k^z} \sigma_k^+ e^{-i\omega_p t \frac{1}{2}\sigma_k^z} \\ &= \sigma_k^+ + \frac{i\omega_p t}{2}\left[\sigma_k^z, \sigma_k^+\right] + \frac{1}{2!}\left(\frac{i\omega_p t}{2}\right)^2 \left[\sigma_k^z, \left[\sigma_k^z, \sigma_k^+\right]\right] + \dots \\ &= \sigma_k^+ \sum_{n=0}^{\infty} \frac{1}{n!}(i\omega_p t)^n = \sigma_k^+ e^{i\omega_p t}, \end{aligned} \tag{A.7}$$

$$\begin{aligned} U_a a\, U_a^\dagger &= e^{i\omega_p t a^\dagger a} a\, e^{-i\omega_p t a^\dagger a} \\ &= a + i\omega_p t\left[a^\dagger a, a\right] + \frac{1}{2!}(i\omega_p t)^2 \left[a^\dagger a, \left[a^\dagger a, a\right]\right] + \dots \\ &= a \sum_{n=0}^{\infty} \frac{1}{n!}(-i\omega_p t)^n = a e^{-i\omega_p t}, \end{aligned} \tag{A.8}$$

and

$$\begin{aligned} U_a a^\dagger U_a^\dagger &= e^{i\omega_p t a^\dagger a} a^\dagger e^{-i\omega_p t a^\dagger a} \\ &= a^\dagger + i\omega_p t\left[a^\dagger a, a^\dagger\right] + \frac{1}{2!}(i\omega_p t)^2 \left[a^\dagger a, \left[a^\dagger a, a^\dagger\right]\right] + \dots \\ &= a^\dagger \sum_{n=0}^{\infty} \frac{1}{n!}(i\omega_p t)^n = a^\dagger e^{i\omega_p t}. \end{aligned} \tag{A.9}$$

Inserting the evaluated terms (A.6)-(A.7) into Equation A.4 and subsequently into Equation A.3 yields the Tavis-Cumming Hamiltonian in the rotating frame

$$\tilde{H} = \Delta_c a^\dagger a + \frac{1}{2}\sum_{k=1}^{N} \Delta_k \sigma_k^z + \sum_{k=1}^{N} g_k\left[\sigma_k^- a^\dagger + \sigma_k^+ a\right] + i\eta(t)\left[a^\dagger - a\right], \tag{A.10}$$

where we introduced the frequency detuning $\Delta_c = \omega_c - \omega_p$ and $\Delta_k = \omega_k - \omega_p$.

Next we want to derive the equations of motions describing the dynamical evolution of the ensemble. We proceed with the Hamiltonian in the rotating frame

Die approbierte gedruckte Originalversion dieser Diplomarbeit ist an der TU Wien Bibliothek verfügbar
The approved original version of this thesis is available in print at TU Wien Bibliothek.

and calculate the equations of motion for the observables a, σ_k^- and σ_k^z using the definition in Equation 2.7 with the Lindblad term defined in Equation 2.6. For the observable a we get

$$\begin{aligned}\frac{d}{dt}\langle a\rangle =& \operatorname{Tr}\left(-i[a,\tilde{H}]\rho + a\mathcal{L}_D[\rho]\right)\\ =& -i\operatorname{Tr}\left(\Delta_c[a,a^\dagger a]\rho + \sum_{k=1}^{N} g_k\left([a,\sigma_k^- a^\dagger] + [a,\sigma_k^+ a]\right)\rho + i\eta(t)\rho\right)\\ &+\kappa\operatorname{Tr}\left[a\left(2a\rho a^\dagger - a^\dagger a\rho - \rho a^\dagger a\right)\right]\\ &+\gamma_h\operatorname{Tr}\left(a\sum_{k=1}^{N}\left(2\sigma_k^-\rho\sigma_k^+ - \sigma_k^+\sigma_k^-\rho - \rho\sigma_k^+\sigma_k^-\right)\right)\\ &+\gamma_p\operatorname{Tr}\left(a\sum_{k=1}^{N}\left(\sigma_k^z\rho\sigma_k^z - \rho\right)\right).\end{aligned} \tag{A.11}$$

The terms proportional to γ_h and γ_p are zero due to the cyclic properties of the trace and the commutators can be evaluated straightforwardly, leading to

$$\begin{aligned}\frac{d}{dt}\langle a\rangle =& -i\operatorname{Tr}\left(\Delta_c a\rho + \sum_{k=1}^{N} g_k\sigma_k^-\rho + i\eta(t)\rho\right)\\ &+\kappa\operatorname{Tr}\left(a\left(2a\rho a^\dagger - a^\dagger a\rho - \rho a^\dagger a\right)\right)\end{aligned} \tag{A.12}$$

With the definition of the expectation value of an observable $\langle O\rangle = \operatorname{Tr}(O\rho)$ and informed algebra we finally arrive at

$$\begin{aligned}\frac{d}{dt}\langle a\rangle =& -i\operatorname{Tr}\left(\Delta_c a\rho\right) - i\sum_{k=1}^{N} g_k\operatorname{Tr}(\sigma_k^-\rho) + \eta(t) + \kappa\operatorname{Tr}\left(-[a,a^\dagger]a\rho\right)\\ =& -(\kappa + i\Delta_c)\langle a\rangle - i\sum_{k=0}^{N} g_k\langle\sigma_k^-\rangle + \eta(t),\end{aligned} \tag{A.13}$$

which resembles the first Maxwell-Bloch equation.

Die approbierte gedruckte Originalversion dieser Diplomarbeit ist an der TU Wien Bibliothek verfügbar
The approved original version of this thesis is available in print at TU Wien Bibliothek.

For the observable σ_k^- we get

$$\begin{aligned}\frac{d}{dt}\langle\sigma_k^-\rangle &= \mathrm{Tr}\left(-i[\sigma_k^-,\tilde{H}]\rho + \sigma_k^-\mathcal{L}_D[\rho]\right)\\ &= -i\,\mathrm{Tr}\left(\frac{1}{2}\sum_{j=1}^{N}\Delta_j[\sigma_k^-,\sigma_j^z]\rho + \sum_{j=1}^{N} g_k\left([\sigma_k^-,\sigma_j^- a^\dagger] + [\sigma_k^-,\sigma_j^+ a]\right)\rho\right)\\ &\quad + \kappa\,\mathrm{Tr}\left(\sigma_k^-\left(2a\rho a^\dagger - a^\dagger a\rho - \rho a^\dagger a\right)\right)\\ &\quad + \gamma_h\,\mathrm{Tr}\left(\sigma_k^-\sum_{j=1}^{N}\left(2\sigma_j^-\rho\sigma_j^+ - \sigma_j^+\sigma_j^-\rho - \rho\sigma_j^+\sigma_j^-\right)\right)\\ &\quad + \gamma_p\,\mathrm{Tr}\left(\sigma_k^-\sum_{j=1}^{N}\left(\sigma_j^z\rho\sigma_j^z - \rho\right)\right),\end{aligned} \tag{A.14}$$

where the term proportional to κ and in the sums over j all terms $j \neq k$ vanish due to the cyclic properties of the trace and the fact that spin operators trivially commute for $j \neq k$. Using the commutation relations (2.2) yields

$$\begin{aligned}\frac{d}{dt}\langle\sigma_k^-\rangle &= -i\Delta_k\,\mathrm{Tr}\left(\sigma_k^-\rho\right) + ig_k\,\mathrm{Tr}\left(\sigma_k^z a\rho\right)\\ &\quad + \gamma_h\,\mathrm{Tr}\left(2\sigma_k^-\sigma_k^-\rho\sigma_k^+ - \sigma_k^-\sigma_k^+\sigma_k^-\rho - \sigma_k^-\rho\sigma_k^+\sigma_k^-\right)\\ &\quad + \gamma_p\,\mathrm{Tr}\left(\sigma_k^-\sigma_k^z\rho\sigma_k^z - \sigma_k^-\rho\right).\end{aligned} \tag{A.15}$$

From the definition of the Pauli matrices we can deduce the relations $\sigma_k^-\sigma_k^- = 0$, $\sigma_k^-\sigma_k^z = \sigma_k^-$ and $\sigma_k^z\sigma_k^- = -\sigma_k^-$, which lets us evaluate the remaining terms

$$\begin{aligned}\frac{d}{dt}\langle\sigma_k^-\rangle &= -i\Delta_k\,\mathrm{Tr}\left(\sigma_k^-\rho\right) + ig_k\,\mathrm{Tr}\left(\sigma_k^z a\rho\right)\\ &\quad + \gamma_h\,\mathrm{Tr}\left(-(\sigma_k^-\sigma_k^+\sigma_k^-\rho + \sigma_k^-\rho\sigma_k^+\sigma_k^-)\right)\\ &\quad + \gamma_p\,\mathrm{Tr}\left(\sigma_k^-\sigma_k^z\rho\sigma_k^z - \sigma_k^-\rho\right)\\ &= -i\Delta_k\,\mathrm{Tr}\left(\sigma_k^-\rho\right) + ig_k\,\mathrm{Tr}\left(\sigma_k^z a\rho\right)\\ &\quad + \gamma_h\,\mathrm{Tr}\left(-(\frac{1}{2}\sigma_k^-\rho + \frac{1}{2}\sigma_k^-\rho)\right)\\ &\quad + \gamma_p\,\mathrm{Tr}\left(-\sigma_k^-\rho - \sigma_k^-\rho\right),\end{aligned} \tag{A.16}$$

yielding the second Maxwell-Bloch equation

$$\frac{d}{dt}\langle\sigma_k^-\rangle = -\left(\gamma_h + 2\gamma_p + i\Delta_k\right)\langle\sigma_k^-\rangle + ig_k\langle\sigma_k^z a\rangle \tag{A.17}$$

Die approbierte gedruckte Originalversion dieser Diplomarbeit ist an der TU Wien Bibliothek verfügbar
The approved original version of this thesis is available in print at TU Wien Bibliothek.
TU Bibliothek Your knowledge hub WIEN

Finally, for the last observable σ_k^z we get

$$\begin{aligned}\frac{d}{dt}\langle\sigma_k^z\rangle &= \mathrm{Tr}\left(-i[\sigma_k^z,\tilde{H}]\rho + \sigma_k^z\mathcal{L}_D[\rho]\right)\\ &= -i\,\mathrm{Tr}\left(\sum_{j=1}^{N} g_j\left([\sigma_k^z,\sigma_j^- a^\dagger] + [\sigma_k^z,\sigma_j^+ a]\right)\rho\right)\\ &\quad + \kappa\,\mathrm{Tr}\left(\sigma_k^z\left(2a\rho a^\dagger - a^\dagger a\rho - \rho a^\dagger a\right)\right)\\ &\quad + \gamma_h\,\mathrm{Tr}\left(\sigma_k^z\sum_{j=1}^{N}\left(2\sigma_j^-\rho\sigma_j^+ - \sigma_j^+\sigma_j^-\rho - \rho\sigma_j^+\sigma_j^-\right)\right)\\ &\quad + \gamma_p\,\mathrm{Tr}\left(\sigma_k^z\sum_{j=1}^{N}\left(\sigma_j^z\rho\sigma_j^z - \rho\right)\right).\end{aligned} \tag{A.18}$$

For the same reasons as mentioned before, all terms in the sums where $k \neq j$ and the term proportional to κ vanish, leaving us with

$$\begin{aligned}\frac{d}{dt}\langle\sigma_k^z\rangle &= -i\,\mathrm{Tr}\left(g_k\left([\sigma_k^z,\sigma_k^- a^\dagger] + [\sigma_k^z,\sigma_k^+ a]\right)\rho\right)\\ &\quad + \gamma_h\,\mathrm{Tr}\left(\sigma_k^z\left(2\sigma_k^-\rho\sigma_k^+ - \sigma_k^+\sigma_k^-\rho - \rho\sigma_k^+\sigma_k^-\right)\right)\\ &\quad + \gamma_p\,\mathrm{Tr}\left(\sigma_k^z\left(\sigma_k^z\rho\sigma_k^z - \rho\right)\right),\end{aligned} \tag{A.19}$$

where we see that the term proportional to γ_p is zero due to the fact that $\sigma_k^z\sigma_k^z = 1$ and the cyclic properties of the trace. Next, we evaluate the commutators and use the relation $\sigma_k^+\sigma_k^- = \frac{1}{2}(\sigma_k^z + 1)$ to find

$$\begin{aligned}\frac{d}{dt}\langle\sigma_k^z\rangle &= -i\,\mathrm{Tr}\left(2g_k\left(-\sigma_k^- a^\dagger + \sigma_k^+ a\right)\rho\right)\\ &\quad + \gamma_h\,\mathrm{Tr}\left(-2\sigma_k^-\rho\sigma_k^+ - \frac{1}{2}\sigma_k^z(\sigma_k^z+1)\rho - \frac{1}{2}\sigma_k^z\rho(\sigma_k^z+1)\right)\\ &= 2ig_k\,\mathrm{Tr}\left(\left(\sigma_k^- a^\dagger - \sigma_k^+ a\right)\rho\right)\\ &\quad + \gamma_h\,\mathrm{Tr}\left(-(\sigma_k^z+1)\rho - \frac{1}{2}(1+\sigma_k^z)\rho - \frac{1}{2}\rho(1+\sigma_k^z)\right),\\ &= 2ig_k\left(\mathrm{Tr}\left(\sigma_k^- a^\dagger\rho\right) - \mathrm{Tr}\left(\sigma_k^+ a\rho\right)\right)\\ &\quad - \gamma_h 2\,\mathrm{Tr}\left((\sigma_k^z+1)\rho\right),\end{aligned} \tag{A.20}$$

which yields the third Maxwell-Bloch equation

$$\frac{d}{dt}\langle\sigma_k^z\rangle = -2\gamma_h\left(\langle\sigma_k^z\rangle + 1\right) + ig_k\left(\langle\sigma_k^- a^\dagger\rangle - \langle\sigma_k^+ a\rangle\right), \tag{A.21}$$

where the last term can be rewritten simply by identifying $\langle\sigma_k^- a^\dagger\rangle = (\langle\sigma_k^+ a\rangle)^*$ to

$$\frac{d}{dt}\langle\sigma_k^z\rangle = -2\gamma_h\left(\langle\sigma_k^z\rangle + 1\right) - 4g_k\,\mathrm{Im}\left(\langle\sigma_k^- a^\dagger\rangle\right). \tag{A.22}$$

Die approbierte gedruckte Originalversion dieser Diplomarbeit ist an der TU Wien Bibliothek verfügbar
The approved original version of this thesis is available in print at TU Wien Bibliothek.
TU Bibliothek Your knowledge hub WIEN

Acknowledgments

I really enjoyed working on this thesis since it enabled me to combine my knowledge in computer science with my physics studies, by simulating the relevant system dynamics and giving the results a physical interpretation.

Unfortunately, due to the Corona virus pandemic, I was not able to meet and exchange with as many clever people at the Rotter group as I would have wished to. Nevertheless, there are a few people I would like to acknowledge and express my deep gratitude to:

- My supervisor Dr. Matthias Zens, who guided me through this work with his immense knowledge on cavity QED. I would especially like to thank him for always being open for questions and helping me out, even after he finished his PhD and left the university.
- My thesis advisor Prof. Stefan Rotter, who provided me a very interesting topic for my master's thesis and who was always open for questions and discussions, deepening my physical understanding.
- The group of Prof. Jörg Schmiedmayer, including Dr. Andreas Angerer, Dipl.-Ing. Wenzel Kersten and Dipl.-Ing. Nikolaus De Zordo, who provided me valuable input and knowledge from the experimentalists' side.
- My parents Karin and Karl Reiter for their unconditional financial and moral support, allowing me to freely pursue my studies.

Die approbierte gedruckte Originalversion dieser Diplomarbeit ist an der TU Wien Bibliothek verfügbar
The approved original version of this thesis is available in print at TU Wien Bibliothek.

Bibliography

[1] E. M. Purcell, "Spontaneous Emission Probabilities at Radio Frequencies," in *Confined Electrons and Photons* (E. Burstein and C. Weisbuch, eds.), vol. 340, pp. 839–839, Boston, MA: Springer US, 1995. Series Title: NATO ASI Series.

[2] S. Haroche and J.-M. Raimond, *Exploring the Quantum*. Oxford University Press, Aug. 2006.

[3] S. Haroche, "Nobel Lecture: Controlling photons in a box and exploring the quantum to classical boundary," *Reviews of Modern Physics*, vol. 85, pp. 1083–1102, July 2013.

[4] D. J. Wineland, "Nobel Lecture: Superposition, entanglement, and raising Schrödinger's cat," *Reviews of Modern Physics*, vol. 85, pp. 1103–1114, July 2013.

[5] E. Jaynes and F. Cummings, "Comparison of quantum and semiclassical radiation theories with application to the beam maser," *Proceedings of the IEEE*, vol. 51, no. 1, pp. 89–109, 1963.

[6] B. W. Shore and P. L. Knight, "The Jaynes-Cummings Model," *Journal of Modern Optics*, vol. 40, pp. 1195–1238, July 1993.

[7] J. H. Eberly, N. B. Narozhny, and J. J. Sanchez-Mondragon, "Periodic Spontaneous Collapse and Revival in a Simple Quantum Model," *Physical Review Letters*, vol. 44, pp. 1323–1326, May 1980.

[8] P. Michler, A. Kiraz, C. Becher, W. V. Schoenfeld, P. M. Petroff, L. Zhang, E. Hu, and A. Imamoglu, "A Quantum Dot Single-Photon Turnstile Device," *Science*, vol. 290, pp. 2282–2285, Dec. 2000.

[9] P. Ginzburg, "Cavity quantum electrodynamics in application to plasmonics and metamaterials," *Reviews in Physics*, vol. 1, pp. 120–139, Nov. 2016.

[10] S. Haroche, M. Brune, and J. M. Raimond, "From cavity to circuit quantum electrodynamics," *Nature Physics*, vol. 16, pp. 243–246, Mar. 2020.

[11] J. M. Raimond, M. Brune, and S. Haroche, "Manipulating quantum entanglement with atoms and photons in a cavity," *Reviews of Modern Physics*, vol. 73, pp. 565–582, Aug. 2001.

Die approbierte gedruckte Originalversion dieser Diplomarbeit ist an der TU Wien Bibliothek verfügbar
The approved original version of this thesis is available in print at TU Wien Bibliothek.

[12] A. Blais, R.-S. Huang, A. Wallraff, S. M. Girvin, and R. J. Schoelkopf, "Cavity quantum electrodynamics for superconducting electrical circuits: An architecture for quantum computation," *Physical Review A*, vol. 69, p. 062320, June 2004.

[13] J. Raimond and G. Rempe, "Cavity Quantum Electrodynamics: Quantum Information Processing with Atoms and Photons," in *Quantum Information* (D. Bruß and G. Leuchs, eds.), pp. 669–689, Wiley, 1 ed., Apr. 2016.

[14] G. Kurizki, P. Bertet, Y. Kubo, K. Mølmer, D. Petrosyan, P. Rabl, and J. Schmiedmayer, "Quantum technologies with hybrid systems," *Proceedings of the National Academy of Sciences*, vol. 112, pp. 3866–3873, Mar. 2015.

[15] Z.-L. Xiang, S. Ashhab, J. Q. You, and F. Nori, "Hybrid quantum circuits: Superconducting circuits interacting with other quantum systems," *Reviews of Modern Physics*, vol. 85, pp. 623–653, Apr. 2013.

[16] H. Mabuchi and A. C. Doherty, "Cavity Quantum Electrodynamics: Coherence in Context," *Science*, vol. 298, pp. 1372–1377, Nov. 2002.

[17] S. Haroche, "Controlling Photons in a Box and Exploring the Quantum to Classical Boundary (Nobel Lecture)," *Angewandte Chemie International Edition*, vol. 52, pp. 10158–10178, Sept. 2013.

[18] Y. Kaluzny, P. Goy, M. Gross, J. M. Raimond, and S. Haroche, "Observation of Self-Induced Rabi Oscillations in Two-Level Atoms Excited Inside a Resonant Cavity: The Ringing Regime of Superradiance," *Physical Review Letters*, vol. 51, pp. 1175–1178, Sept. 1983.

[19] M. Brune, F. Schmidt-Kaler, A. Maali, J. Dreyer, E. Hagley, J. M. Raimond, and S. Haroche, "Quantum Rabi Oscillation: A Direct Test of Field Quantization in a Cavity," *Physical Review Letters*, vol. 76, pp. 1800–1803, Mar. 1996.

[20] H. J. Kimble, "Strong Interactions of Single Atoms and Photons in Cavity QED," *Physica Scripta*, vol. T76, no. 1, p. 127, 1998.

[21] R. J. Thompson, G. Rempe, and H. J. Kimble, "Observation of normal-mode splitting for an atom in an optical cavity," *Physical Review Letters*, vol. 68, pp. 1132–1135, Feb. 1992.

[22] R. Chikkaraddy, B. de Nijs, F. Benz, S. J. Barrow, O. A. Scherman, E. Rosta, A. Demetriadou, P. Fox, O. Hess, and J. J. Baumberg, "Single-molecule strong coupling at room temperature in plasmonic nanocavities," *Nature*, vol. 535, pp. 127–130, July 2016.

Die approbierte gedruckte Originalversion dieser Diplomarbeit ist an der TU Wien Bibliothek verfügbar
The approved original version of this thesis is available in print at TU Wien Bibliothek.
TU Bibliothek Your knowledge hub WIEN

[23] K. Santhosh, O. Bitton, L. Chuntonov, and G. Haran, "Vacuum Rabi splitting in a plasmonic cavity at the single quantum emitter limit," *Nature Communications*, vol. 7, p. ncomms11823, Sept. 2016.

[24] A. Wallraff, D. I. Schuster, A. Blais, L. Frunzio, R.-S. Huang, J. Majer, S. Kumar, S. M. Girvin, and R. J. Schoelkopf, "Strong coupling of a single photon to a superconducting qubit using circuit quantum electrodynamics," *Nature*, vol. 431, pp. 162–167, Sept. 2004.

[25] J. M. Fink, M. Göppl, M. Baur, R. Bianchetti, P. J. Leek, A. Blais, and A. Wallraff, "Climbing the Jaynes–Cummings ladder and observing its nonlinearity in a cavity QED system," *Nature*, vol. 454, pp. 315–318, July 2008.

[26] D. Najer, I. Söllner, P. Sekatski, V. Dolique, M. C. Löbl, D. Riedel, R. Schott, S. Starosielec, S. R. Valentin, A. D. Wieck, N. Sangouard, A. Ludwig, and R. J. Warburton, "A gated quantum dot strongly coupled to an optical microcavity," *Nature*, vol. 575, pp. 622–627, Nov. 2019.

[27] Y. Kubo, F. R. Ong, P. Bertet, D. Vion, V. Jacques, D. Zheng, A. Dréau, J.-F. Roch, A. Auffeves, F. Jelezko, J. Wrachtrup, M. F. Barthe, P. Bergonzo, and D. Esteve, "Strong Coupling of a Spin Ensemble to a Superconducting Resonator," *Physical Review Letters*, vol. 105, p. 140502, Sept. 2010.

[28] R. Amsüss, C. Koller, T. Nöbauer, S. Putz, S. Rotter, K. Sandner, S. Schneider, M. Schramböck, G. Steinhauser, H. Ritsch, J. Schmiedmayer, and J. Majer, "Cavity QED with Magnetically Coupled Collective Spin States," *Physical Review Letters*, vol. 107, p. 060502, Aug. 2011.

[29] K. Sandner, H. Ritsch, R. Amsüss, C. Koller, T. Nöbauer, S. Putz, J. Schmiedmayer, and J. Majer, "Strong magnetic coupling of an inhomogeneous nitrogen-vacancy ensemble to a cavity," *Physical Review A*, vol. 85, p. 053806, May 2012.

[30] S. Putz, D. Krimer, R. Amsüss, A. Valookaran, T. Nöbauer, J. Schmiedmayer, S. Rotter, and J. Majer, "Protecting a spin ensemble against decoherence in the strong-coupling regime of cavity QED," *Nature Physics*, vol. 10, pp. 720–724, Oct. 2014.

[31] D. O. Krimer, S. Putz, J. Majer, and S. Rotter, "Non-Markovian dynamics of a single-mode cavity strongly coupled to an inhomogeneously broadened spin ensemble," *Physical Review A*, vol. 90, p. 043852, Oct. 2014.

[32] A. Angerer, S. Putz, D. O. Krimer, T. Astner, M. Zens, R. Glattauer, K. Streltsov, W. J. Munro, K. Nemoto, S. Rotter, J. Schmiedmayer, and J. Majer, "Ultralong relaxation times in bistable hybrid quantum systems," *Science Advances*, vol. 3, p. e1701626, Dec. 2017.

Die approbierte gedruckte Originalversion dieser Diplomarbeit ist an der TU Wien Bibliothek verfügbar
The approved original version of this thesis is available in print at TU Wien Bibliothek.
TU Bibliothek Your knowledge hub WIEN

[33] F. Campaioli, F. A. Pollock, and S. Vinjanampathy, "Quantum Batteries," in *Thermodynamics in the Quantum Regime* (F. Binder, L. A. Correa, C. Gogolin, J. Anders, and G. Adesso, eds.), vol. 195, pp. 207–225, Cham: Springer International Publishing, 2018. Series Title: Fundamental Theories of Physics.

[34] F. Pirmoradian and K. Mølmer, "Aging of a quantum battery," *Physical Review A*, vol. 100, p. 043833, Oct. 2019.

[35] R. H. Dicke, "Coherence in Spontaneous Radiation Processes," *Physical Review*, vol. 93, pp. 99–110, Jan. 1954.

[36] C. Greiner, B. Boggs, and T. W. Mossberg, "Superradiant Emission Dynamics of an Optically Thin Material Sample in a Short-Decay-Time Optical Cavity," *Physical Review Letters*, vol. 85, pp. 3793–3796, Oct. 2000.

[37] J. G. Bohnet, Z. Chen, J. M. Weiner, D. Meiser, M. J. Holland, and J. K. Thompson, "A steady-state superradiant laser with less than one intracavity photon," *Nature*, vol. 484, pp. 78–81, Apr. 2012.

[38] B. Julsgaard and K. Mølmer, "Dynamical evolution of an inverted spin ensemble in a cavity: Inhomogeneous broadening as a stabilizing mechanism," *Physical Review A*, vol. 86, p. 063810, Dec. 2012.

[39] M. O. Scully and M. S. Zubairy, *Quantum optics*. Cambridge; New York: Cambridge University Press, 1997.

[40] D. F. Walls and G. J. Milburn, *Quantum Optics*. Berlin, Heidelberg: Springer-Verlag Berlin Heidelberg Springer e-books, 2008.

[41] D. A. Redman, S. Brown, R. H. Sands, and S. C. Rand, "Spin dynamics and electronic states of N-V centers in diamond by EPR and four-wave-mixing spectroscopy," *Physical Review Letters*, vol. 67, pp. 3420–3423, Dec. 1991.

[42] M. W. Doherty, N. B. Manson, P. Delaney, F. Jelezko, J. Wrachtrup, and L. C. Hollenberg, "The nitrogen-vacancy colour centre in diamond," *Physics Reports*, vol. 528, pp. 1–45, July 2013.

[43] M. Tavis and F. W. Cummings, "Exact Solution for an N - Molecule—Radiation-Field Hamiltonian," *Physical Review*, vol. 170, pp. 379–384, June 1968.

[44] J. Dukelsky, S. Pittel, and G. Sierra, "*Colloquium* : Exactly solvable Richardson-Gaudin models for many-body quantum systems," *Reviews of Modern Physics*, vol. 76, pp. 643–662, Aug. 2004.

Die approbierte gedruckte Originalversion dieser Diplomarbeit ist an der TU Wien Bibliothek verfügbar
The approved original version of this thesis is available in print at TU Wien Bibliothek.
TU Bibliothek Your knowledge hub WIEN

[45] O. Babelon and D. Talalaev, "On the Bethe ansatz for the Jaynes–Cummings–Gaudin model," *Journal of Statistical Mechanics: Theory and Experiment*, vol. 2007, pp. P06013–P06013, June 2007.

[46] O. Tsyplyatyev, J. von Delft, and D. Loss, "Simplified derivation of the Bethe-ansatz equations for the Dicke model," *Physical Review B*, vol. 82, p. 092203, Sept. 2010.

[47] W. Pogosov, D. Shapiro, L. Bork, and A. Onishchenko, "Exact solution for the inhomogeneous Dicke model in the canonical ensemble: Thermodynamical limit and finite-size corrections," *Nuclear Physics B*, vol. 919, pp. 218–237, June 2017.

[48] H.-P. Breuer and F. Petruccione, *The Theory of Open Quantum Systems*. Oxford University Press, Jan. 2007.

[49] H. J. Carmichael, *Statistical Methods in Quantum Optics 1: Master Equations and Fokker-Planck Equations*. Texts and Monographs in Physics, Berlin: Springer, 1999.

[50] G. S. Agarwal, *Quantum optics*. Cambridge, UK: Cambridge University Press, 2013.

[51] K. Henschel, J. Majer, J. Schmiedmayer, and H. Ritsch, "Cavity QED with an ultracold ensemble on a chip: Prospects for strong magnetic coupling at finite temperatures," *Physical Review A*, vol. 82, p. 033810, Sept. 2010.

[52] H. A. M. Leymann, A. Foerster, and J. Wiersig, "Expectation value based equation-of-motion approach for open quantum systems: A general formalism," *Physical Review B*, vol. 89, p. 085308, Feb. 2014.

[53] S. Krämer and H. Ritsch, "Generalized mean-field approach to simulate the dynamics of large open spin ensembles with long range interactions," *The European Physical Journal D*, vol. 69, p. 282, Dec. 2015.

[54] M. Sánchez-Barquilla, R. E. F. Silva, and J. Feist, "Cumulant expansion for the treatment of light–matter interactions in arbitrary material structures," *The Journal of Chemical Physics*, vol. 152, p. 034108, Jan. 2020.

[55] M. Kira and S. W. Koch, *Semiconductor Quantum Optics*. Cambridge: Cambridge University Press, 2011.

[56] R. Bonifacio and G. Preparata, "Coherent Spontaneous Emission," *Physical Review A*, vol. 2, pp. 336–347, Aug. 1970.

Die approbierte gedruckte Originalversion dieser Diplomarbeit ist an der TU Wien Bibliothek verfügbar
The approved original version of this thesis is available in print at TU Wien Bibliothek.
TU Bibliothek Your knowledge hub WIEN

[57] M. Zens, D. O. Krimer, and S. Rotter, "Critical phenomena and nonlinear dynamics in a spin ensemble strongly coupled to a cavity. II. Semiclassical-to-quantum boundary," *Physical Review A*, vol. 100, p. 013856, July 2019.

[58] R. Kubo, "Generalized Cumulant Expansion Method," *Journal of the Physical Society of Japan*, vol. 17, pp. 1100–1120, July 1962.

[59] T. Mori, "Exactness of the mean-field dynamics in optical cavity systems," *Journal of Statistical Mechanics: Theory and Experiment*, vol. 2013, p. P06005, June 2013.

[60] H. Primakoff and T. Holstein, "Many-Body Interactions in Atomic and Nuclear Systems," *Physical Review*, vol. 55, pp. 1218–1234, June 1939.

[61] A. Angerer, S. Putz, D. O. Krimer, T. Astner, M. Zens, R. Glattauer, K. Streltsov, W. J. Munro, K. Nemoto, S. Rotter, J. Schmiedmayer, and J. Majer, "Dynamical Exploration of Amplitude Bistability in Engineered Quantum Systems," *Science Advances*, vol. 3, p. e1701626, Dec. 2017. arXiv: 1703.04779.

[62] T. Astner, J. Gugler, A. Angerer, S. Wald, S. Putz, N. J. Mauser, M. Trupke, H. Sumiya, S. Onoda, J. Isoya, J. Schmiedmayer, P. Mohn, and J. Majer, "Solid-state electron spin lifetime limited by phononic vacuum modes," *Nature Materials*, vol. 17, pp. 313–317, Apr. 2018.

[63] B. Julsgaard and K. Mølmer, "Fundamental limitations in spin-ensemble quantum memories for cavity fields," *Physical Review A*, vol. 88, p. 062324, Dec. 2013.

[64] W.-l. Song, W.-l. Yang, Z.-q. Yin, C.-y. Chen, and M. Feng, "Controllable quantum dynamics of inhomogeneous nitrogen-vacancy center ensembles coupled to superconducting resonators," *Scientific Reports*, vol. 6, p. 33271, Dec. 2016.

[65] S. Putz, *Circuit Cavity QED with Macroscopic Solid-State Spin Ensembles*. Springer Theses, Recognizing Outstanding Ph.D. Research, Cham: Springer International Publishing : Imprint: Springer, 1st ed. 2017 ed., 2017.

[66] W. H. Press, ed., *Numerical recipes: the art of scientific computing*. Cambridge, UK ; New York: Cambridge University Press, 3rd ed ed., 2007. OCLC: ocn123285342.

[67] C. Tsallis, S. V. F. Levy, A. M. C. Souza, and R. Maynard, "Statistical-Mechanical Foundation of the Ubiquity of Lévy Distributions in Nature," *Physical Review Letters*, vol. 75, pp. 3589–3593, Nov. 1995.

Die approbierte gedruckte Originalversion dieser Diplomarbeit ist an der TU Wien Bibliothek verfügbar
The approved original version of this thesis is available in print at TU Wien Bibliothek.
TU Bibliothek Your knowledge hub WIEN

[68] D. Prato and C. Tsallis, "Nonextensive foundation of Lévy distributions," *Physical Review E*, vol. 60, pp. 2398–2401, Aug. 1999.

[69] B. S. Goh, "Global Stability in Many-Species Systems," *The American Naturalist*, vol. 111, pp. 135–143, Jan. 1977.

[70] G. Floquet, "Sur les équations différentielles linéaires à coefficients périodiques," *Annales scientifiques de l'École normale supérieure*, vol. 12, pp. 47–88, 1883.

[71] F. Bloch, "Über die Quantenmechanik der Elektronen in Kristallgittern," *Zeitschrift für Physik*, vol. 52, pp. 555–600, July 1929.

[72] A. A. Svidzinsky, X. Zhang, and M. O. Scully, "Quantum versus semiclassical description of light interaction with atomic ensembles: Revision of the Maxwell-Bloch equations and single-photon superradiance," *Physical Review A*, vol. 92, p. 013801, July 2015.

[73] B. Rose, A. Tyryshkin, H. Riemann, N. Abrosimov, P. Becker, H.-J. Pohl, M. Thewalt, K. Itoh, and S. Lyon, "Coherent Rabi Dynamics of a Superradiant Spin Ensemble in a Microwave Cavity," *Physical Review X*, vol. 7, p. 031002, July 2017.

[74] M. Zens and S. Rotter, "Superabsorption by time-reversing superradiance," *Nature Photonics*, vol. 15, pp. 251–252, Apr. 2021.

[75] B. C. Hall, *Lie groups, Lie algebras, and representations: an elementary introduction*. No. 222 in Graduate texts in mathematics, Cham; New York: Springer, second edition ed., 2015. OCLC: ocn910324548.

Die approbierte gedruckte Originalversion dieser Diplomarbeit ist an der TU Wien Bibliothek verfügbar
The approved original version of this thesis is available in print at TU Wien Bibliothek.